Robotics and Autonomous Systems 70 (2015) 126–144

Contents lists available at ScienceDirect

Robotics and Autonomous Systems

journal homepage: www.elsevier.com/locate/robot

An autonomous all terrain robotic system for field demining missions

David Portugal *, Gonçalo Cabrita, Bruno D. Gouveia, David C. Santos, José A. Prado

Instituto de Sistemas e Robótica (ISR), Universidade de Coimbra (UC), 3030-290 Coimbra, Portugal

HIGHLIGHTS

- Proposal of a new affordable, lightweight and autonomous all-terrain robot for demining operations.
- Complete description of the mechanical system and design of the modular robotic architecture.
- Validation of the robot's intelligent capabilities in outdoor experiments.
- Work in progress and lessons learned for minefield coverage, and mine detection.

ARTICLE INFO

Article history:
Received 13 November 2014
Received in revised form
16 February 2015
Accepted 27 February 2015
Available online 9 March 2015

Keywords:
Robotic system architecture
Field and Service Robotics
Humanitarian demining

ABSTRACT

Mines deployed in post-war countries pose severe threats to civilians and hamper the reconstruction effort in war hit societies. In the scope of the EU FP7 TIRAMISU Project, a toolbox for humanitarian demining missions is being developed by the consortium members. In this article we present the FSR Husky, an affordable, lightweight and autonomous all terrain robotic system, developed to assist human demining operation teams. Intended to be easily deployable on the field, our robotic solution has the ultimate goal of keeping humans away from the threat, safeguarding their lives. A detailed description of the modular robotic system architecture is presented, and several real world experiments are carried out to validate the robot's functionalities and illustrate continuous work in progress on minefield coverage, mine detection, outdoor localization, navigation, and environment perception.

1. Introduction

The removal of landmines has become a global emergency. According to UNICEF, over 100 million landmines are still lodged in the ground worldwide, harming and taking lives of over 20 thousand people every year, the vast majority civilians. Battlefield debris like landmines and other unexploded ordnance (UXO) may remain active for decades, posing an eminent risk for local people. In addition, they hamper peace-keeping, stability and reconstruction efforts, preventing the recovery of nations, inhibiting the use of land for food production, and not allowing refugees to return home. On the other hand, demining is a time-consuming, stressful, tiresome and dangerous task, and it costs hundreds of times more than setting mines. It requires complete removal of all mines buried in the field so that the land can be returned to the local population, and there is an imperative need to improve safety, reliability and speed of demining operations [1]. The objective of the EU FP7 Toolbox Implementation for Removal of Anti-Personnel Mines, Submunitions and UXO (TIRAMISU[1]) project is to provide the mine action community with a toolbox to assist in addressing the several issues related to humanitarian demining, thus promoting peace, national and regional security, conflict prevention, social and economic rehabilitation and post-conflict reconstruction [2]. In this context, the Institute of Systems and Robotics of the University of Coimbra (ISR-UC), is the project consortium member responsible for developing robotics research tools for field demining operations, and landmine sensor detection.

There have been important advances related to technology for mine detection and removal over the past decades. As a robotic application, mine clearance and removal is challenging and risky, however it has tremendous potential. Besides increasing safety for human deminers, robotic systems should increase productivity by speeding up the process. Moreover, these systems should be able to distinguish landmines from other buried debris, while being sensitive to all types of explosive devices. In terms of operation in the field, a demining robot must maneuver continuously for long

* Corresponding author.
E-mail addresses: davidbsportugal@sapo.pt (D. Portugal), goncabrita@isr.uc.pt (G. Cabrita), bgouveia@isr.uc.pt (B.D. Gouveia), david.sc.santos@isr.uc.pt (D.C. Santos), jaugusto@isr.uc.pt (J.A. Prado).

http://dx.doi.org/10.1016/j.robot.2015.02.013
0921-8890/

[1] http://www.fp7-tiramisu.eu.

Fig. 1. The FSR Husky demining robot.

periods of time in widely varying environment conditions and terrains over large areas. This assumes robustness against vibration, as well as easiness of maintenance and field deployment, leveraging from a flexible, modular and reliable design. Further relevant aspects include intuitive human–machine interface with real-time interaction, the possibility to remotely control the robot within safe distances, and a portable, fast-response and reliable mine detecting system [1]. Having this in mind, in this work we describe the development of an autonomous lightweight all terrain robot for field demining missions in the framework of the EU FP7 TIRAMISU Project—the FSR Husky (*cf.* Fig. 1). In addition to the description and integration of the robotic system, our focus is also placed on its intelligent functionalities such as outdoor localization, navigation, environment perception, and its potential for application in minefield coverage, and mine detection as reported by outdoor field trials.

In the remainder of this article, an overview of related work in the area of robotic tools and sensors in mine clearance operations is presented. Afterwards, in Section 3 we describe in detail the development and assembling of our robotic system, providing information on hardware components, sensor specifications, kinematics, software integration, development, and testing. In the subsequent section, we validate the robot's intelligent capabilities by means of several field trials, discuss results, and report important lessons learned during the ICRA 2014 Humanitarian Robotics and Automation Technology Challenge (HRATC 2014)[2] that we have organized under the endorsement of the IEEE Robotics and Automation Society—Special Interest Group on Humanitarian Technology (IEEE RAS-SIGHT). Finally, the article ends with concluding considerations and future research directions.

2. Related work

Robotic tools developed so far for demining purposes have focused in a variety of aspects, *e.g.* modular mine detection payloads for existing demining robots [3], blast resistant armored systems that deal with vegetation clearance and mine removal [4], remotely controlled lightweight robot systems [5], semi-autonomous especially designed robots [6], and even suspended pole robots [7]. The proposed robotic systems in the literature differ in terms of speed, level of autonomy, operation time, mine detection technology, locomotion and mobility, weight, size, payload, capabilities, cost, and robustness. Below, we review important work in this area, with special focus on demining robots, mine sensing technology and field coverage.

Several field robots have been presented in the academic research context over the last decades. Gryphon-IV [8] developed in the Tokyo Institute of Technology, is a large four-wheeler all-terrain vehicle that can be remotely controlled or manually driven from the inside. It has a long-reach 3 m wide manipulator with a non-metallic pantograph arm with 3 degrees of freedom (DOF), which is equipped with a Ground Penetrating Radar (GPR) and a conventional Metal Detector (MD). In addition to the long range WiFi, the robot is endowed with a pair of stereo cameras, being capable of modeling the terrain for traversal, and it uses Global Positioning System (GPS) for outdoor localization. Being built around an all-terrain buggy, the robot runs on gasoline with a 25 L tank, which corresponds to an operation time of around 10 h, and the robot's maximum payload is 170 kg. According to [9], since 2005 its capabilities have been evaluated in several prepared test-minefields with deactivated landmines, enduring most weather conditions, and terrain configurations, and allowing to gradually improve the various aspects of the robot.

Following a distinct philosophy, researchers from the University of Genova have been developing a four wheeled agricultural tractor with blast resistant wheels against anti-personnel (AP) mines, named LOw COSt TRActor for humanitarian demining (LOCOSTRA) [10]. The system is built around a commercially available tractor with a 50 L diesel tank combined with converted off-the-shelf agricultural tools, being able to cut through vegetation and prepare the ground before mine removal, with its excavation system. The main goal is to reduce deminer accidents and increase the clearance speed in a cost-effective way. Similarly to Gryphon-IV, LOCOSTRA is also not fully autonomous and must be remotely teleoperated. The key innovation is the thick steel armored wheels which are designed to withstand the forces associated with an anti-personnel mine detonation, allowing the machine to continue to work if it inadvertently detonates a mine. The overall weight of the tractor is around 1850 kg, and it can traverse uneven and steep ground due to its articulated skid-steering, with a lift capacity of 1800 kg. The cost has been kept below €50,000. Field tests in the Jordan–Syria border have shown that LOCOSTRA is blast resistant up to 280 g of Trinitrotoluene (TNT), and it is easy to use by an untrained remote operator [11].

Researchers from the Royal Military Academy (RMA) of Belgium have also been working on a heavy tracked outdoor Explosive Ordnance Disposal (EOD) platform called tEODor [12]. This 350 kg robotic system is endowed with electronics, sensors, computing power, motor control units and power sources in order to be able to execute remote controlled and semi-autonomous tasks. In terms of mine detection, it is equipped with a Multi-Channel system with 5 independent MDs. Additionally, the robot includes an active vision system consisting in a Time-of-Flight (TOF) camera, and a stereo camera, mounted on a pan–tilt unit [13], giving the robot further capabilities such as terrain traversability analysis. Remote-operation functionalities are provided via an intuitive human–machine interface (HMI). The platform runs on lead-gel rechargeable batteries with a continuous operation time between 2 and 3 h. Field experiments have proven the usefulness of the tEODor platform in dealing with rough terrain, with good maneuverability and off-road performance. Moreover, the rugged design of the platform makes it capable of handling unfriendly environmental conditions which is crucial for demining tasks.

Most likely inspired by the 2-bicycle-wheel PErsonal Mine EXplorer (PEMEX) robot, proposed by Nicoud and Habib during the nineties [14], researchers from the University of Lisbon have developed an affordable robotic vehicle with four independently steered bicycle wheels, named Ares [15]. The robot presents a behavior-based control system, allowing it to have four different locomotion modes (turning-point, lateral, displacement and double Ackerman). Powered by lead–acid batteries that provide 4 h of operation

[2] http://isr.uc.pt/HRATC2014.

time, Ares uses stereo vision as its primary sensory modality, and is equipped with a low cost compass. Thus, localization is obtained by fusing visual odometry, wheel odometry, and magnetometer and accelerometer information. The platform is also equipped with bumpers and sonars for obstacle detection, and allegedly an odor sensor is used for TNT explosive detection. However, there were no reports of the successful application of this sensor found, neither of fully autonomous operation of the robot in field trials.

Field conditions may limit the progress of humanitarian missions. Thus, several authors highlight the potential of a walking solution in order to adapt to unstructured natural environments, *e.g.* [16]. In the work of Gonzalez de Santos et al. [17], a six-legged robot for humanitarian demining missions, named SILO-6 is proposed. This hexapod possesses a 5 DOF scanning manipulator, which handles a sensor head consisting of a metal detector, infrared sensors and a set of flex sensors. In terms of localization, the robot provides odometry information from the joint-positioning sensors, absolute orientation around the vertical axis from an electromagnetic compass, and differential GPS. These three sources of localization are fused using a Kalman Filter (KF). The control modes of the system are mainly teleoperation and operator-in-the-control-loop, and its operation time is over 1 h on DC batteries. Furthermore, SILO-6 is limited to a maximum speed of 0.5 m/s. In fact, wheeled and tracked vehicles are often preferred by the field robotics community, due to the low speed, complexity, weight and cost involved in most walking robots [18].

In alternative to complete robotic systems for mine clearance such as the aforementioned ones, some research groups have focused on modular payload units for existing military robots such as the Niitek Minestalker, the iRobot Packbot or the Foster-Miller Talon [19–21] reportedly with successful field deployment. Following a modular approach, these payloads can be deployed across multiple robots and extend the native abilities of existing robotic platforms without substantial re-engineering efforts. These include threat detection payloads (*e.g.* sweeping mechanisms, manipulators, excavation systems, explosive detectors), marking system payloads (*e.g.* multi-color paint system, flag deployment), navigation payloads (*e.g.* lasers, camera, GPS, IMU), and the controller unit payload (*e.g.* onboard CPU, Ethernet communication, USB interface) [3]. For more details in robotics for humanitarian demining, a thorough survey on this issue is available in [6].

From within the available mine sensing technologies, the most widely used is still the MD, which is based on the principle of electromagnetic induction. MDs have been enhanced over the years to enable background rejection so as to avoid false alarms due to metal fragments. They usually have small dimensions, low weight, low energy consumption and low cost. However, they may suffer from limitations related to the magnetic properties of the soil, concentration of metal scraps, burial depth of mines and mines with minimal metal composition [22,23]. Advances in geophysical technologies have enabled the utilization of subsurface imaging. Particularly, Ground Penetrating Radars (GPRs) have been employed in the field with promising results [24]. This technology is useful for the discrimination of targets, enabling the visualization of their shape [25] up to 30 cm of depth, albeit their sensitiveness to heterogeneous soil moisture. GPR works by emitting an electromagnetic wave into the ground using an antenna which does not need direct ground contact. In order to overcome the limitations of MDs and GPR, and explore their complementary features, it is also common to combine both sensors in a dual configuration. Such solutions require methods for data fusion and are commonly employed in a hand-held device or vehicle, *e.g.* [26,27]. Several other technologies have been proposed and discussed in the literature, presenting different levels of technological maturity, such as vapor explosive detection systems based on chemical sensors, passive microwave radiometers, thermal, multi-spectral and acoustic imaging systems, photo-acoustic spectroscopy, X-ray backscatter techniques, nuclear quadropole resonance (NQR), thermal and fast neutron analysis (TNA & FNA), multi-sensor probes with force and tactile feedback, and others [28].

Despite recent advances, the development of a unique robot that can operate under all terrain and environmental conditions while meeting all demining requirements is not a simple task [6]. In their current status, robotized solutions are often expensive, unsafe, complex and inflexible [29], and are still best used as mobile platforms endowed with arrays of mine detection sensors with restricted decision-making capabilities. Nevertheless, a recognized effort has been made by several research groups to design autonomous robots in order to eliminate the permanent presence of an operator. While heavy-duty mine clearance vehicles were popular as an alternative to manual demining, nowadays the focus has been put on developing small and cheaper mobile demining robots that can deal with confined spaces, and without having logistical problems associated with transportation to remote areas [19]. Similarly, the development of deformable machines that can get through narrow entrances has been discussed, e.g. [18], and the literature is consensual in pointing out that robots should follow modular mechanical structures, by separating mobility from manipulation and focusing on improving current robot platforms [6,7,29]. These machines can also be used in cooperation with dog teams and/or manual clearance teams, as well as unmanned aerial vehicles (UAVs), which may enhance localization, reconnaissance, trajectory planning and communications in rough environments, and also provide wide-area assessment [29]. Besides, swarm robotics is also attractive seeing as multiple, small and low-cost robots can coordinate their actions in the field, while speeding up the process and sharing experience on the identification of mines [19].

Robots for humanitarian demining usually start their missions along the boundaries of the minefield, with the detection sensors placed above the terrain inside. Over the course of the mission, the robot slowly progresses inside according to the degree of belief on the absence of mines in the minefield [18]. Thus, fully autonomous robots can benefit from intelligent coverage strategies [30]. In the particular case of mine clearance, the goal of the robot is not to detect an opponent inside a closed area. Unlike classical robotic coverage [31], this means that the robot trajectory does not have to be necessarily optimal in terms of distance covered, and possible constraints such as being unpredictable by an external observer, or not knowing the shape of the area prior to the mission do not apply. The key aspect in minefield coverage is to guarantee that all the area is scanned for mines, hence the robot may not need to physically go everywhere as long as its detection system (*e.g.* sensing arm) covers the entire area. In addition, in minefield coverage it is desirable to respect an optimization criteria such as minimizing coverage time or being energy-efficient. For example, Jin and Tang [32] consider terrain elevation and the effect of slopes in their coverage strategy, while Oksanen and Visala [33] follow a split-and-merge strategy to decompose the area in simpler convex polygons, which can then be traversed following a lawn mowing trajectory. Furthermore, the coverage problem may also be extended to teams of robots working in parallel, in order to reduce mission time [34,35].

2.1. Statement of contributions

In this work, we present an all-terrain robotic platform named FSR Husky, for field demining missions. Our philosophy differs from the previously referred robots, by presenting an affordable lightweight system with autonomous capabilities such as outdoor navigation, localization and perception, which uses a clearance arm to detect and localize landmines in a suspicious area. Despite

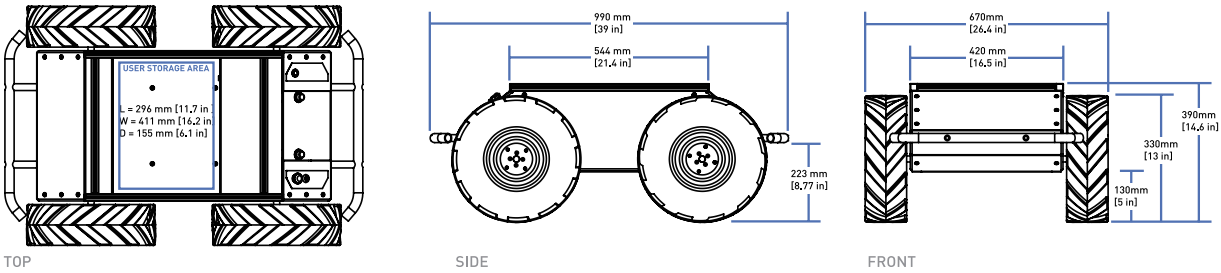

Fig. 2. Husky robot base dimensions.

its humanitarian relevance and the numerous works addressing this topic in the past years, this is still an open problem without an affordable commercial solution. We describe the implementation, features, and modular integration of the robotic system together with details on its capabilities, and foreseen development, so as to achieve full autonomy. Field trials validate the work conducted, and their outcome allows for a discussion of the potential to employ the robot in demining operations. We also discuss lessons learned during the HRATC 2014 competition, and outline future directions of research in this area.

3. The FSR Husky platform

In this section we describe the components of the proposed all-terrain robotic system, focusing especially on its steering base, hardware and sensors, robot kinematics and constraints, energy consumption, arm sweeping for mine coverage, software, and testing tools.

3.1. Robot base

The FSR Husky is built around a Clearpath Husky A200 robot base.[3] This is a rugged yet compact, 50 kg lightweight all-terrain vehicle for field robotics research. With an International Protection (IP) rating of IP55, it is fully protected against splash water from any direction, and dust, thus not interfering with the correct operation of the equipment. The Husky dimensions can be found in Fig. 2. With a width of almost 1 m and a generous amount of ground clearance, the vehicle is able to get over large obstacles with ease, due to its 330 mm lug tread tires with high-torque 4 × 4 drive, which provide great traction and minimize slip. Thus, the Husky A200 is suitable for traversing extreme terrains, operating with confidence in sand, snow, mud and dirt. Being a skid steered vehicle, the robot base does not have axles connecting the left and right wheels. Instead, the two wheels on one side are connected and rotate independently of the other side, similarly to tracked vehicles. The difference in rotation causes the vehicle to skid and turn in the direction of the slower wheels. Skid steered systems have greater traction on the surface, being particularly suited for rough terrains. However, the performance of the vehicle strongly depends on the surface of the terrain and speed of the vehicle, since skidding may cause unpredictable power requirements because of terrain irregularities and nonlinear tire–soil interaction. We address the power model issue later in Section 3.4.

The base platform includes front and rear bumper bars, which can act as secondary payload mount or used to lift and transport the robot. In terms of speed and performance, the robot base withstands a maximum payload of 75 kg over challenging outdoor terrains, reaching speeds of up to 1.0 m/s, and being able to climb slopes of up to 45°. The Husky base is equipped with high-resolution quadrature encoders with 200.000 pulse/m. It can be controlled using multiple options such as direct voltage, wheel speed or kinematic velocity, providing the flexibility for specific research objectives and application requirements. Control can easily be performed using LabView, C++, Python and the Robot Operating System (ROS). In this work, the ROS drivers will be used as the adopted standard (*cf.* Section 3.6). Using the extruded aluminum payload mounting rail, and the ample internal user space, the robot presents great flexibility for incorporating further hardware, as seen in the next subsection.

3.2. Hardware and sensors

The FSR Husky is comprised of several sensors and hardware. Most hardware is placed inside the ample user storage area (*cf.* Fig. 3(a)), and most sensors are mounted on top of the elevated device mounting structures (EDMSs) that were placed above the aluminum rail of the robot base, as illustrated in Fig. 3(b). Below, we describe the modules that integrate the proposed demining robot platform, and causing its overall price to remain below €30,000.

A diagram of all the modules, which illustrates how they communicate and how they are powered is presented in Fig. 4. The robot is powered by a single 24 V, 20 Ah sealed lead–acid battery, capable of delivering 1800 W, which is placed in the battery compartment on the rear chassis of the robot. The user outputs provided are 5 V, 12 V, and 24 V fused at 5 A each. Additionally, the Husky A200 base provides a RS232 Connector for serial port communication, which interfaces with the remaining hardware via a USB-serial adapter that we have connected to an Anker USB 3.0 9 Port Hub.

Regarding sensors, two PointGrey Flea3 GigE cameras are placed over the front EDMS to provide real-time imaging in the field with a resolution of 1288 × 964 at 30 frames per second (FPS) and equipped with C-mount lenses. These cameras are mounted on ball joints on top of rails that allow adjusting the baseline and camera orientation. A wide variety of computer vision algorithms [36] can be used to perform different tasks in the field such as stereo reconstruction, visual odometry localization, tracking of the clearance mine detecting systems, detecting trails and obstacles, and more.

Additionally, an Xsens MTi-300 Inertial Measurement Unit (IMU) containing gyroscopes, accelerometers and magnetometers, provides 3D orientation, acceleration and rate of turn to the FSR Husky. This component features vibration-rejecting gyroscopes and a novel sensor fusion algorithm that overcomes limitations in Kalman filtering, named Xsens Estimation Engine (XEE). It also has a 1.0° accuracy in roll, pitch and yaw measurements. This equipment enables us to track the robot orientation in 3D, and can optionally be used to control and stabilize the cameras.

A very useful sensor for outdoor navigation is a Global Positioning System (GPS) unit. The FSR Husky is equipped with the u-blox NEO-6P GPS, which combines the high performance of

[3] http://www.clearpathrobotics.com/husky/features.

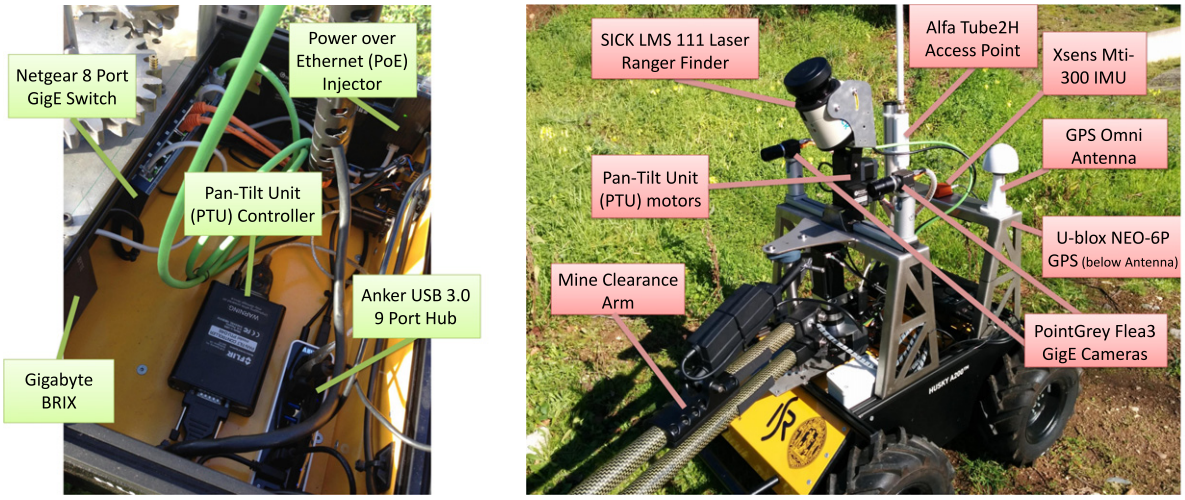

(a) Robot hardware inside the storage area.

(b) Sensors and hardware mounted on top of the robot base.

Fig. 3. Hardware and sensors of the FSR Husky.

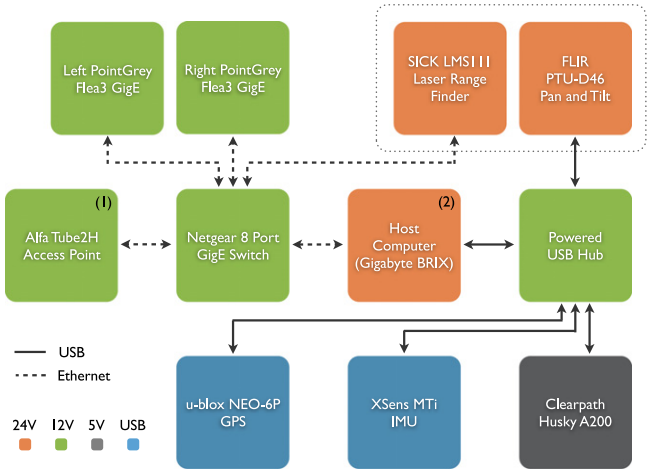

Fig. 4. The FSR Husky schematic. (1) The Alfa Tube2H is powered over a PoE module. (2) The BRIX is powered over a 19 V DC/DC converter.

Fig. 5. The GPS-RTK reference base station.

the u-blox 6 position engine with Precise Point Positioning (PPP) technology. It yields extremely high levels of position accuracy in static and slow moving applications. The GPS unit is attached on the rear EDMS, being connected to an omnidirectional antenna. In order to further improve the estimation of latitude and longitude derived from GPS, we also have the possibility to use Real-Time Kinematic (RTK) satellite navigation, to provide global positioning with centimeter-level accuracy. To this end, the FSR Husky needs a reference base station, as shown in Fig. 5. The base station is placed on a single reference point, providing real-time correction to the robot by re-broadcasting the phase of the carrier that it observes. The robot then compares its own phase measurements with the one received from the base station, allowing it to calculate their relative position. Our base station is composed of a tall tripod and a housing containing the base station receiver, which communicates via USB with a base station computer that relays the raw GPS data to the robot via WiFi. Later in Section 4.1, we describe the localization system, which combines the GPS, IMU and Odometry outputs in an Extended Kalman Filter (EKF).

Another key sensor incorporated in the FSR Husky is the SICK LMS111 Laser Range Finder (LRF). This is a commonly used sensor in Robotics for distance sensing, obstacle detection, navigation and mapping. It scans the environment using laser beams to determine the distance to objects and build 2D representations of the environment. The maximum range of the SICK LMS111 is 20 m at 50 Hz, with a field of view (FOV) of 270° and a resolution between 0.25° and 0.5°. The SICK laser, which weights 1.1 kg is mounted on a FLIR PTU-D46 pan and tilt that allows for the laser to produce point clouds of 3D space instead of only a 2D scan slice. The pan and tilt unit (PTU) is designed for high-speed, accurate positioning of lasers up to 2.7 kg at speeds up to 300°/s, with 0.051° of resolution.

In terms of communication, an 8 port Netgear GS108T-200 Gigabit Ethernet (GigE) switch with a 16 Gbps full duplex bandwidth provides Ethernet interface, and the aforementioned powered USB 3.0 hub at 5 Gbps provides USB interface. These two modules are in charge of internal communication, enabling the interaction between all sensors and hardware of the robot. Communication to the outside is accomplished using an Alfa Tube 2H access point. The AlfaTube 2H is an outdoor WiFi access point, which is equipped with a 2.4 GHz and 9 dBi long range outdoor omnidirectional Antenna, being placed on the rear EDMS. This equipment enables the persistent connection of the robot to an external computer (usually the base station computer), receiving feedback and retrieving field data for online and offline analysis.

The host computer chosen to process all data and run the developed software is the ultra compact Gigabyte BRIX. The small-sized computer easily sits in the palm of one's hands without compromising raw power, with an Intel Core i7-3537U at 3.1 GHz,

Fig. 6. Robot mine clearance arm with the Vallon VMP3 metal detector.

8 GB DDR3 RAM and a 60 GB solid-state disk (SSD). The BRIX includes a DC IN connection, USB 3.0, and GigE ports, used to power the BRIX over a 19 V DC/DC converter, and connect it to the Anker USB hub and Netgear switch. The BRIX is placed inside the storage area, which is spacious enough to fit further sensors and hardware, depending on the application.

Finally, the mobile robot is equipped with a landmine detecting sensor attached to an actuator arm. The chosen sensor for detecting AP mines is a Vallon VMP3 three-coil, pulse induction MD. The Vallon VMP3 was modified to fit in the robotic arm of the FSR Husky. The MD is mainly composed by two parts: (1) the antenna which is attached to the arm and; (2) the SPU (Signal Processing Unit) which is fitted to the back of the robot under the EDMS holding the WiFi and GPS antennas. The Vallon VMP3 can be powered using the USB charging port and its processing unit contains a serial port, which makes it possible to read the output (NMEA readable text datasets) by establishing a link between the MD and a computer via a RS232 interface at 115.2 kbit/s. Each coil provides 3 channels of data at a rate of 10 Hz, thus the total data flows at a rate of 30 Hz.

The MD is mounted on a 2 DOF robotic arm that sweeps the detector above the ground. The mine clearance arm gives the robot the ability to move the metal detector antenna from side to side as well as to lift it or bring it closer to the soil. The arm is mounted at the front of the FSR Husky, as depicted in Fig. 6. The mine clearance arm works by controlling the Nanotec PD4-N60, which is a high-pole DC servo motor based on a stepper motor. The motor is programmable, being ideal for distributed or multi-axis application. In order to interface with the linear actuator of the arm so as to control it, we use a Pololu Jrk 21v3 motor controller with feedback. The auxiliary serial port of the Pololu Jrk is used to communicate with the Nanotec PD4-N60 via a RS485 serial communication interface. Furthermore, an integrated reduction gear with 1:15 gear ratio, and a second stage with 1:1.67 gear ratio, enable the motor to maintain a high torque. The arm has 0.85 m of length from the drive shaft to the center of the coil, it is composed of carbon and polyamide parts and non-metallic material both to reduce the overall weight and prevent any interference with the metal detector. Additionally it can be swept up to 180° in the horizontal plane, with a maximum end effector height of 580 mm and minimum height of −180 mm. As safety interlock, a limit switch is placed on the largest cogwheel to guarantee the full 180° of arm's motion, with a single Hall effect sensor and two magnets.

3.3. Kinematics

A wheeled robot usually has several motors where each one rotates a wheel. The velocity of the ith wheel is defined as $V_i = \rho\omega_i$,

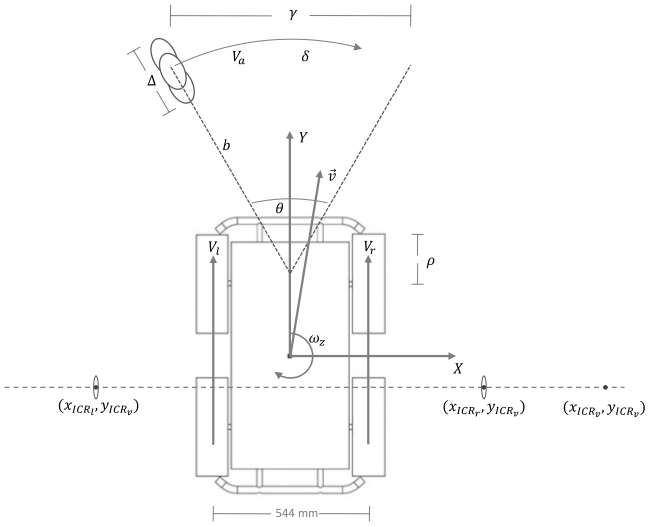

Fig. 7. Kinematics of the FSR Husky robotic platform.

where ρ is the wheel's radius and ω_i is the respective motor's angular velocity. Similarly, the velocity of the arm sweeping is given by $V_a = b\omega_a$, where b is the length of the arm and ω_a is the angular velocity of the arm motor. Dynamic models for skid-steering may result too costly for real-time motion control and dead-reckoning. Bearing this in mind, we make use of known geometric relationships since it has been shown that the movement of these type of vehicles can be estimated accurately using knowledge of the Instantaneous Center of Rotation (ICR) locations [37,38]. We assume that the ground mobile robot moves in 2D space in a skid-steering configuration, meaning that the wheels do not steer, the distance between wheels and the distance between axes are always the same, and the velocities of the two wheels on the same side of the robot are equivalent, similarly to a tracked robot. Thus, it is possible to represent the robot's velocity by three variables: v_x, v_y, and ω_z, where $v = (v_x, v_y)$ is the vehicle's translational velocity with respect to its local frame (with the Y axis aligned with the forward motion direction), and ω_z is its angular velocity.

Let V_l, and V_r represent the linear velocities of the left and right pair of wheels respectively. Then, direct kinematics can be stated as:

$$\begin{pmatrix} v_x \\ v_y \\ \omega_z \end{pmatrix} = A \cdot \begin{pmatrix} V_l \\ V_r \end{pmatrix}. \tag{1}$$

In order to obtain the kinematic relation matrix A, we follow the procedure described in [39] by using knowledge of the ICR locations. Considering the local coordinates shown in Fig. 7, the ICR of the vehicle during rotation is expressed as $ICR_v = (x_{ICR_v}, y_{ICR_v})$, and the ICRs for the left and right wheels are defined as: $ICR_l = (x_{ICR_l}, y_{ICR_v})$ and $ICR_r = (x_{ICR_r}, y_{ICR_v})$. Note that the y_{ICR_v} coordinate is common to the three points, since they lie on a parallel line to the local X axis. The geometrical relation between the ICR locations, the vehicle velocity, and the wheels velocity is:

$$x_{ICR_v} = -\frac{v_y}{\omega_z}, \tag{2}$$

$$x_{ICR_l} = \frac{\alpha_l \cdot V_l - v_y}{\omega_z}, \tag{3}$$

$$x_{ICR_r} = \frac{\alpha_r \cdot V_r - v_y}{\omega_z}, \tag{4}$$

$$y_{ICR_v} = \frac{v_x}{\omega_z}. \tag{5}$$

The nominal wheel speeds are affected by correction factors (α_l, α_r), which account for mechanical issues such as tire inflation conditions. These values should ideally be close to 1. However, they can be adjusted by measuring the actual traveled distance by the robot in straight motion or more precisely with other experimental setups such as those described in [39]. The values of x_{ICR_v} range within $[-\infty, +\infty]$. However, the values of x_{ICR_l}, x_{ICR_r}, and y_{ICR_v} remain bounded. This boundedness is limited to the case of kinematic motion, in which centrifugal dynamics are neglected and slippage is due only to steering. Thus, by manipulating Eqs. (3)–(5), we obtain the following relationships:

$$v_x = -\frac{-y_{ICR_v} \cdot \alpha_l \cdot V_l + y_{ICR_v} \cdot \alpha_r \cdot V_r}{x_{ICR_r} - x_{ICR_l}}, \tag{6}$$

$$v_y = -\frac{x_{ICR_r} \cdot \alpha_l \cdot V_l - x_{ICR_l} \cdot \alpha_r \cdot V_r}{x_{ICR_r} - x_{ICR_l}}, \tag{7}$$

$$\omega_z = -\frac{-\alpha_l \cdot V_l + \alpha_r \cdot V_r}{x_{ICR_r} - x_{ICR_l}}. \tag{8}$$

Finally, the general kinematic relation matrix A is given by:

$$A = \frac{1}{x_{ICR_r} - x_{ICR_l}} \cdot \begin{bmatrix} -y_{ICR_v} \cdot \alpha_l & y_{ICR_v} \cdot \alpha_r \\ x_{ICR_r} \cdot \alpha_l & -x_{ICR_l} \cdot \alpha_r \\ -\alpha_l & \alpha_r \end{bmatrix}. \tag{9}$$

3.4. Energy consumption

The FSR Husky sealed lead–acid battery allows the robot to operate continuously around 3 h. Real-time monitoring of the instantaneous robot power consumption is available using the provided software. As a consequence, we have implemented a power estimation model according to key physical motion variables. To this end, let us consider that $Pm(\omega, \theta)$ is the consumption of a motor moving at angular velocity ω, and with angular acceleration $\theta = \frac{d\omega}{dt}$. According to [40], a polynomial fitting is a good approach to model the power of the motors since the behavior of these can be represented by an unbounded function. In [41], the power model of a basic motor was modeled as a second-degree polynomial of ω, in [42] it was shown that a sixth degree model would be more suitable. From the experimental data collected, *e.g.* Fig. 8, we find that a machine learning approach is more realistic. Therefore we have trained a Bayesian network with four leaf nodes: acceleration—*acc*, jerk—*jer*, angular velocity—*vel*, and robot pitch—*pit* (acquired by the IMU unity mounted on the robot). The influence of each variable was trained into the Bayesian network using datasets acquired in field tests with our robot. The power model can be expressed, applying Bayes rule as:

$$P(kW|acc, vel, jer, pitch) = \frac{P(acc|kW) \cdot P(vel|kW) P(jer|kW) \cdot P(pit|kW) \cdot P(kW)}{P(acc, vel, jer, pit)}, \tag{10}$$

wherein we assume that there is no prior information about the robot's power. Hence, the prior factor $P(kW)$ is defined as uniform. As for the likelihood distributions modeling the variables according to power, these were obtained by training the Bayesian Network, and are presented in Fig. 9. Additionally, the denominator term $P(acc, vel, jer, pitch)$ is regarded as a normalization factor, being often omitted for simplification purposes [43]. A comparison between the measured power and the estimated power by our model in a typical robot run is shown in Fig. 10. The mean absolute error of the estimation is $\varepsilon = 0.0078$ kW.

Moreover, once considering that the model presented in Fig. 10 is the power model of the wheels' motors (P_{mw}), in a similar manner we found the power model of the arm motor P_{ma}; and the power consumption cost function of the robot can be defined as:

$$\sum_{i=1}^{4} P_{mw}\left(\omega_{wi}, \frac{d\omega_{wi}}{dt}\right) + P_{ma}\left(\omega_a, \frac{d\omega_a}{dt}\right). \tag{11}$$

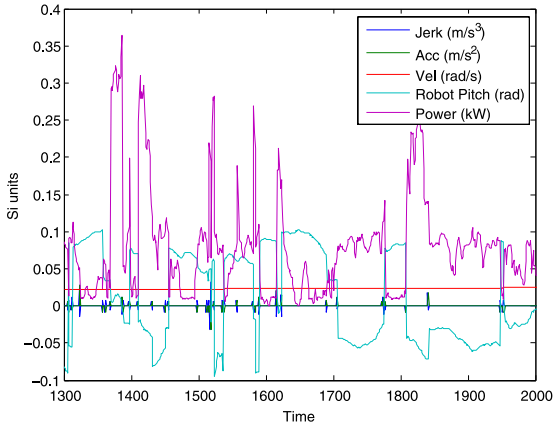

Fig. 8. Data collected from the robot during a field trial.

3.5. Arm sweeping

In this section, we address the problem of optimizing the combined motion of the mobile platform with the mine clearance arm. Refer to Fig. 11 and let θ be the range of rotation of the arm. The arc traveled by the sensor is $\delta = \theta \cdot b$, thus with the robot stopped during a full arm sweep the sensor travels 2δ. Let Δ be the length of the sensor, in order to cover all the ground without gaps. The maximum distance that the robot can move forward during a full arm sweep that takes t seconds is Δ. Considering that the arm angular velocity is given by:

$$\omega_a = \frac{2\theta}{t}. \tag{12}$$

We can relate ω_a with the robot's maximum linear velocity $v_{\max}$ by:

$$v_{\max} = \frac{\Delta}{t} \Rightarrow v_{\max} = \frac{\Delta \omega_a}{2\theta}. \tag{13}$$

Besides, this shows that even though we could set $\theta = \pi$, which is the maximum range of rotation supported by the mine clearance arm, when moving forward the arm angle of sweeping (θ) affects the maximum velocity of the robot so as to guarantee a full area coverage with minimal overlap.

Case Study. In our robot, each coil of the metal detector is equipped with one chemical sensor, so the arm sweeping movement generates simultaneously 3 lines of dual data. These dual sensor data is fused and interpolated based on the method proposed in [26], and generates an arc strip of covered area in front of the robot with length Δ (see Fig. 11). The application of optimizing the motion of the platform with the sweeping arm in our case yields the following constraints:

- The length of the dual sensor is $\Delta = 0.62$ m.
- The width of the arm is $b = 0.85$ m.
- The minimum width of the covered strip γ is equal to the robot's width, *i.e.* $\gamma_{\min} = 0.67$ m.
- According to the MD's documentation, the linear velocity of the arm V_a should be limited to $1/2$ m/s. The study presented in [44] confirms that this value is the maximum acceptable speed for proper sensor functionality.

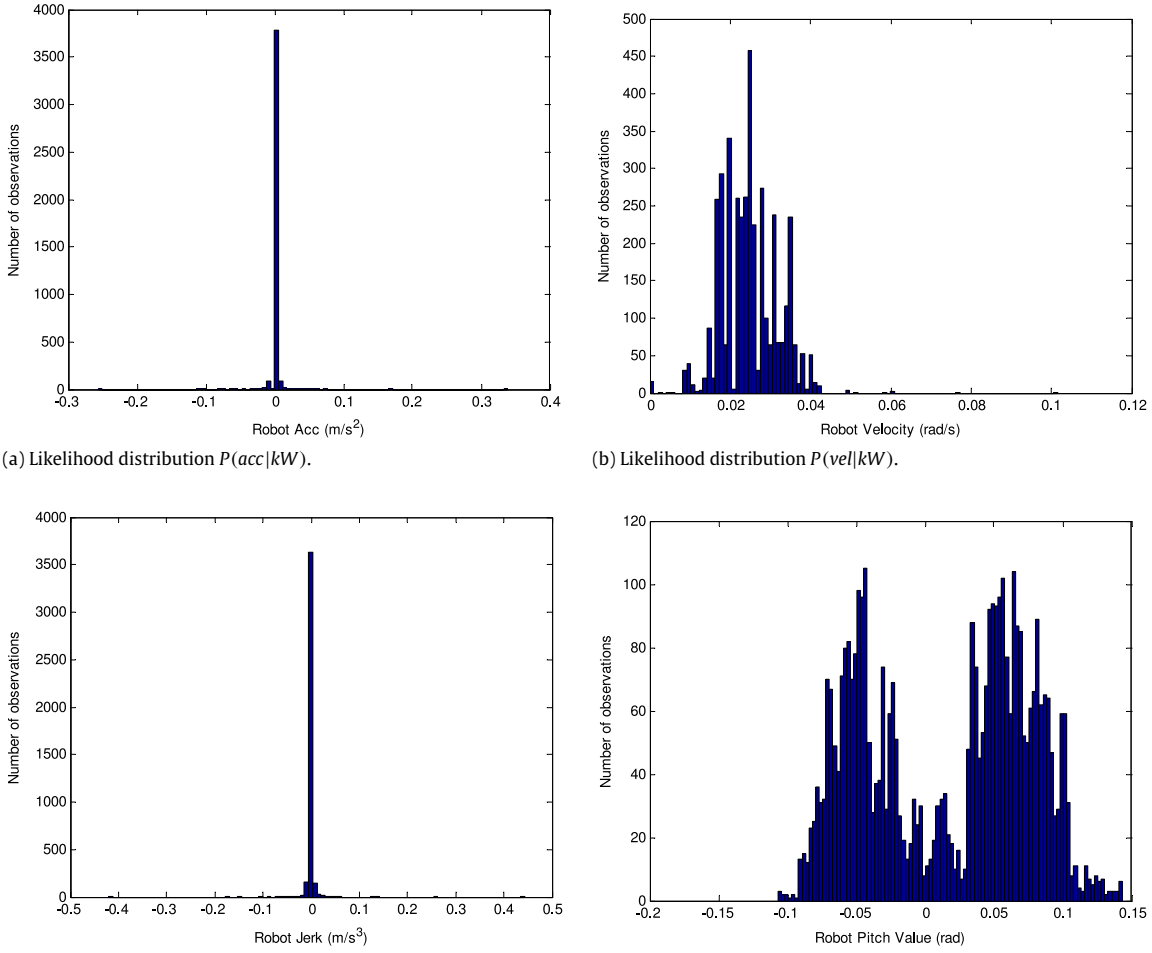

(a) Likelihood distribution $P(acc|kW)$.

(b) Likelihood distribution $P(vel|kW)$.

(c) Likelihood distribution $P(jer|kW)$.

(d) Likelihood distribution $P(pit|kW)$.

Fig. 9. Likelihood distribution of the significant variables of the proposed power model.

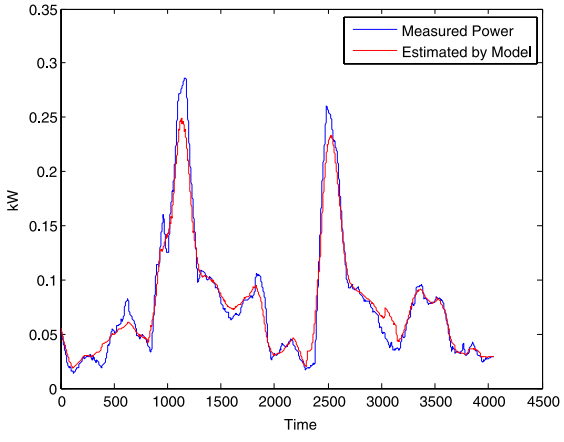

Fig. 10. Comparison between measured power and estimated by the proposed model.

Considering these constraints, the maximal angular velocity of the arm is given by:

$$\omega_a = \frac{V_a}{b} \Rightarrow \omega_a = \frac{0.5}{0.85} = 0.588\,\text{rad/s}. \tag{14}$$

Therefore, relationship (13), becomes:

$$v_{\max} = \frac{0.62 \times 0.588}{2\theta} \Rightarrow v_{\max} = \frac{0.182}{\theta}. \tag{15}$$

As referred before, the maximum range of rotation of the arm is $\theta_{\max} = \pi$, and the minimal range is given by:

$$\tan\left(\frac{\theta_{\min}}{2}\right) = \frac{\gamma_{\min}/2}{b} = 0.3941, \tag{16}$$

$$\begin{aligned}\frac{\theta_{\min}}{2} &= \arctan(0.3941)\\ &= 0.3754\,\text{rad} \Rightarrow \theta_{\min} = 0.7508\,\text{rad}\,(43.02^\circ).\end{aligned} \tag{17}$$

By setting the range of rotation of the arm $\theta \in [0.7508, \pi]$, we can use (15) to extract the theoretically optimal linear velocity of the robot that guarantees that the arm scan will perform without gaps. Below some indicative values of θ, and the corresponding $v_{\max}$ are presented:

$\theta = \pi/4\,(45^\circ)$, $\quad v_{\max} = 0.232\,\text{m/s}.$
$\theta = \pi/3\,(60^\circ)$, $\quad v_{\max} = 0.174\,\text{m/s}.$
$\theta = \pi/2\,(90^\circ)$, $\quad v_{\max} = 0.116\,\text{m/s}.$
$\theta = \pi\,(180^\circ)$, $\quad v_{\max} = 0.058\,\text{m/s}.$

It is our belief that the sweeping arm will not pose severe constraints on the coverage algorithm, apart from the maximum velocity that the robot can travel in order to guarantee that the area is covered by rely on several turns in place are not advised so as to avoid redundant and inefficient coverage.

3.6. Software and ROS integration

Despite the existence of many different robotic frameworks that were developed in the last decade, ROS [45] has already

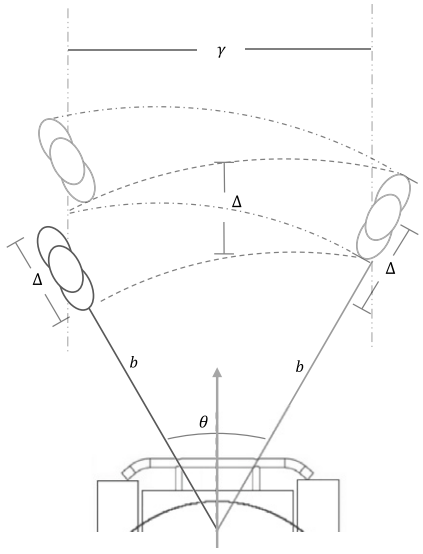

Fig. 11. Combined robotic movement and arm sweeping.

become the most trending and popular robotic framework, being used worldwide due to a series of features that it encompasses and being the closest one to become the *de facto* standard that the robotics community urgently needed. The required effort to develop any robotic application can be daunting, as it must contain a deep layered structure, starting from driver-level software and continuing up through perception, abstract reasoning and beyond. Robotic software architectures must also support large-scale software integration efforts. Therefore, usually roboticists end up spending excessive time with engineering solutions for their particular hardware setup [46]. In the past, many robotic researchers solved some of those issues by presenting a wide variety of frameworks to manage complexity and facilitate rapid prototyping of software for experiments, thus resulting in several robotic software systems currently used in academia and industry. Those frameworks, such as *Player* [47] or *CARMEN* [48], were designed in response to perceived weaknesses of other available frameworks or to place emphasis on aspects which were seen as most important in the design process. ROS is the product of trade-offs and prioritizations made during this process.

The major goals of ROS are hardware abstraction, low-level device control, implementation of commonly-used functionalities, message-passing between processes and package management. ROS promotes code reuse with different hardware by providing a large amount of libraries available for the community, as well as tools for 3D visualization (*rviz*), recording experiments and playing back data offline (*rosbag*), and much more. Regular updates enable the users to obtain, build, write, test and run ROS code, even across multiple computers, given its support for many processors running distributedly. Additionally, since it is highly flexible, with a simple architecture, ROS allows reusing code from numerous other open-source projects, such as Stage [49], Gazebo [50], Open Source Computer Vision—OpenCV [51], and others. As a result, integrating robots and sensors in ROS is highly beneficial, since it strongly reduces the development time.

The FSR Husky is fully integrated in the ROS framework. The software has been developed in C++ programming language using the stable distribution ROS Hydro, and the code is free and open-source.[4] Fortunately, ROS provides seamless integration of new sensors without needing hardware expertise, thus we make use of several drivers available by the ROS community for common sensors, such as the Xsens Mti-300 IMU and the SICK LMS 111 LRF, as well as Clearpath's driver for the robot base, which greatly reduced the overall time spent in developing software. As for the other sensors, ROS drivers have been developed for the PointGrey GigE cameras, the FLIR Pan–Tilt Unit D46, the Vallon VMP3 MD, and the u-blox NEO-6P GPS, which is compatible with rtklib[5] for precise point positioning through RTK-GPS. The implementation of such drivers place virtually all complexity in libraries, only creating small executables, *i.e.* ROS nodes, which expose library functionalities to ROS.

Given that the whole system is the result of an integration of several different modules, when starting up the robot it will automatically check which components are plugged in and start their respective driver, which become responsible for publishing sensor data in dedicated ROS topics. The robot's communication light on the rear panel will change from red to green, indicating that ROS is up and has established communications with the FSR Husky. Note that all the software is run in the onboard computer Gigabyte BRIX. Typically, we establish a connection by WiFi to an external computer in order to run the ROS 3D visualizator, *rviz* (*cf.* Fig. 12), for diagnostics and checking the correct operation of all modules.

Besides the integration of the sensors in ROS, we have also developed a teleoperation node to drive the robot around, because in order to lift the robot using the front and rear bars, at least two people are necessary. Teleoperation is particularly useful to park the robot or to test its functionalities in a specific place. To this end, we use a Xbox joystick, which can communicate with the robot in ranges up to 9 m via a wireless gaming receiver adapter that is connected in the USB hub inside the robot. The teleoperation node can multiplex any navigation software being run on the robot, meaning that while driving autonomously, if the remote control is used, autonomous navigation is interrupted. This concept is shown in Fig. 13.

During the development phase of intelligent robotic algorithms, it is important to continuously test various aspects of the approach. Additionally, it may not be always possible to conduct field trials due to weather conditions, maintenance, etc. Therefore, the robot should be mimicked using a realistic simulation-based tool, which provides training to the developers and operators in nominal and extreme situations, reducing the chances of erroneous behavior in the real field. Having this in mind, we use the 3D Gazebo simulator as illustrated in Fig. 14 to model, to some extent, the robot's dynamics and kinematics, terrain, robot–terrain interactions, and landmine detection sensors. Noise modeling is considered in all sensors of the robot, which in turn are simulated in Gazebo. We have specified white noise for every sensor, defined according to their datasheets. The simulator is configured just like the real robot, which means that a program that runs in Gazebo also runs in the real robot without modifications, and from our experience generally the output is similar in both the virtual and the real world, except for a few issues that are reported in Section 5.2.

In the next section, we describe intelligent capabilities like localization, navigation, perception, and mine detection, which underpin the use of the robot in outdoor demining missions.

4. Robot capabilities

4.1. Extended Kalman Filter (EKF) for localization

Aiming to achieve robust autonomous navigation in unstructured outdoor environments, a set of sensors has been selected to be integrated in this work:

[4] Available at: https://github.com/goncabrita/fsr_husky.

[5] http://www.rtklib.com.

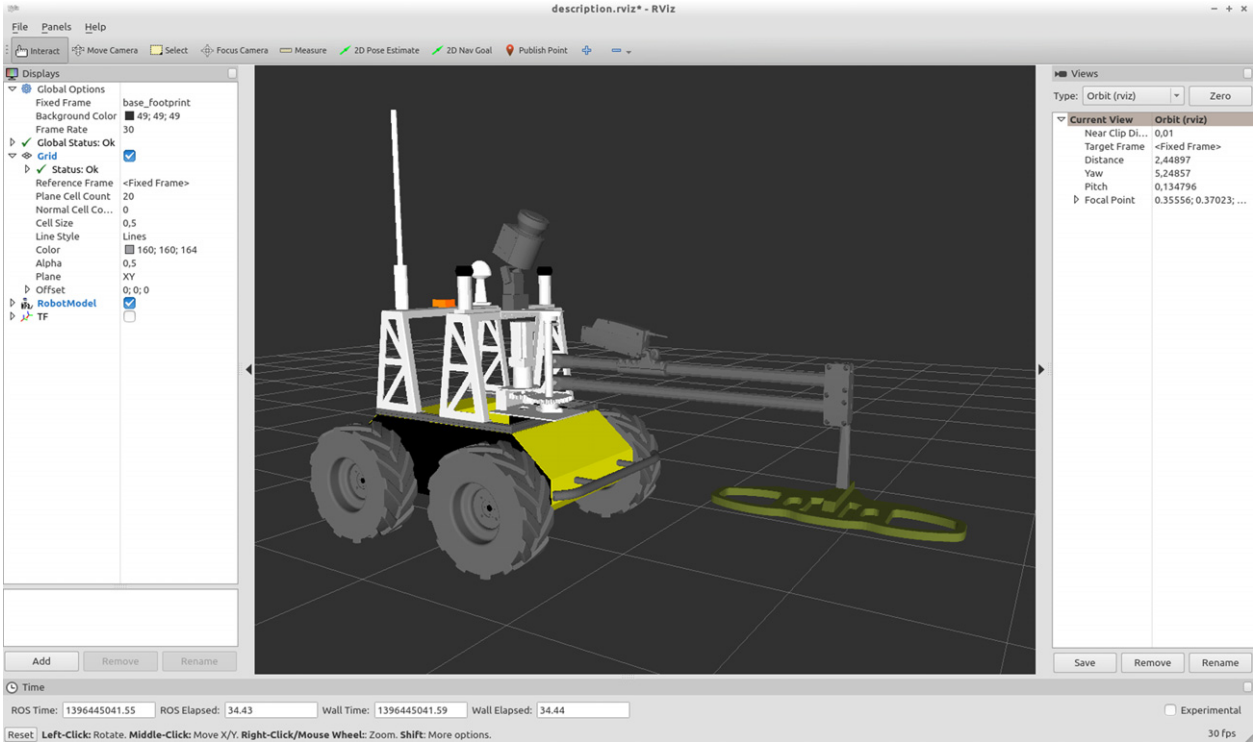

Fig. 12. The FSR Husky robot model on *rviz*.

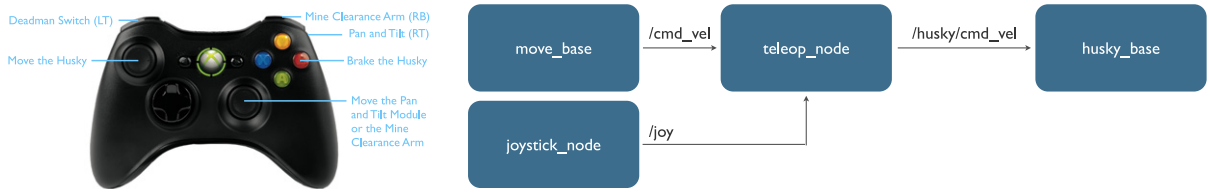

(a) Xbox Joystick to control the FSR Husky.

(b) Multiplexed Teleoperation Scheme.

Fig. 13. Teleoperation of the FSR Husky.

- Inertial Measurement Unit (composed by accelerometers, magnetometers, gyrometers),
- Global Positioning System (RTK-GPS one at base station, another at the rover),
- Robot Wheel Odometry.

Theoretically it is possible to perform IMU-only based localization. However, the accelerometers cannot distinguish between acceleration induced by gravity and acceleration caused by other forces over the vehicle body. Thus, in practice unbounded errors are inevitable during long term operation. Often a GPS receiver is used to correct the estimates provided by the IMU. On the other hand, GPS receivers may temporarily fail due to weather and environmental conditions, *e.g.* tree shadows and clouds. The use of data from motion sensors to calculate the robot's position is widely known as Odometry estimation. In wheeled robots, a series of measurements of the rotations of the wheels can be used to track the robot's 2D pose (x, y, ψ). In the case of skid-steering robots such as the FSR Husky, they usually exhibit agile maneuverability to the extent of turning in place, about their center of gravity. However, when compared to other steering methods, they are not so accurate, since the wheels that are skidding are not tracking the exact movement of the robot. Hence, odometry estimation accumulates error over operation time especially in rough terrains. Nevertheless, in short sampling intervals, particularly during straight motion or when the quality of the received GPS signal is low, odometry can be a precious input for the localization estimation. The literature regarding IMU/GPS/Odometry integration is extensive, *cf.* [52,53].

In the proposed 6D localization system (3D position and 3D orientation) we make use of a classical Extended Kalman Filter (EKF), which is an adaptation of the ROS Robot Pose EKF implementation,[6] considering the IMU and GPS as absolute measurement sensors. The filter has the following discrete time, nonlinear stochastic model:

$$\mathbf{x}_k = f(\mathbf{x}_{k-1}, \mathbf{u}_{k-1}) + \mathbf{w}_{k-1}, \tag{18}$$

$$\mathbf{y}_k = h(\mathbf{x}_k) + \mathbf{v}_k, \tag{19}$$

with $\mathbf{x} \in \mathbb{R}^n$, $\mathbf{u} \in \mathbb{R}^m$ and $\mathbf{y} \in \mathbb{R}^p$ being state, input and measurement variables. It is assumed that $\mathbf{w}_k$ and $\mathbf{v}_k$ are uncorrelated, gaussian random noise, with zero mean and $\mathbf{Q}_k$ and $\mathbf{R}_k$ covariance matrices. They model uncertainty on process and measurement models given by Eqs. (18) and (19), respectively. $\mathbf{u}_k^T$ represents the measurements provided by IMU and $f(\cdot, \cdot)$ represents a discrete time transition function. $\mathbf{x}_k$ is the system state space variable at discrete time $t_k = kT$, with T being the IMU sampling period. In the measurement process (19), both measurement $\mathbf{y}_k$ and function $h(\cdot)$

[6] http://wiki.ros.org/robot_pose_ekf.

Fig. 14. 3D Gazebo simulation of the FSR Husky in an outdoor environment.

change according to which measurement is available at time t_k. In this work, three independent types of observations are considered: direct measurement of the vehicle's 3D orientation given by IMU (φ, θ, ψ), GPS 3D position measurements (x, y, z), and Odometry 2D pose measurements (x, y, ψ). The sources operate at different rates and with different latencies, continuously providing an estimate of the covariance on the measurement.

Regarding the implementation of our specific filter, the covariances are provided by the sensor drivers used. These can either be static matrices, *e.g.* IMU, or dynamic over time according to the extracted measurements, which is the case for GPS and Odometry readings.

In particular, the XSens MTi-300 IMU covariance is:

$$\mathbf{R}^{IMU} = \begin{pmatrix} \sigma^2_{\varphi\varphi} & \sigma^2_{\varphi\theta} & \sigma^2_{\varphi\psi} \\ \sigma^2_{\theta\varphi} & \sigma^2_{\theta\theta} & \sigma^2_{\theta\psi} \\ \sigma^2_{\psi\varphi} & \sigma^2_{\psi\theta} & \sigma^2_{\psi\psi} \end{pmatrix} = \begin{pmatrix} 0.0174 & 0 & 0 \\ 0 & 0.0174 & 0 \\ 0 & 0 & 0.1571 \end{pmatrix}. \quad (20)$$

The Odometry covariance differs when the robot is in motion (*OdomM*), or when it is stopped (*OdomS*). Namely:

$$\mathbf{R}^{OdomM} = \begin{pmatrix} \sigma^2_{xx} & \sigma^2_{xy} & \sigma^2_{x\psi} \\ \sigma^2_{yx} & \sigma^2_{yy} & \sigma^2_{y\psi} \\ \sigma^2_{\psi x} & \sigma^2_{\psi y} & \sigma^2_{\psi\psi} \end{pmatrix} = \begin{pmatrix} 0.001 & 0 & 0 \\ 0 & 0.001 & 0 \\ 0 & 0 & 10^6 \end{pmatrix}, \quad (21)$$

$$\mathbf{R}^{OdomS} = \begin{pmatrix} \sigma^2_{xx} & \sigma^2_{xy} & \sigma^2_{x\psi} \\ \sigma^2_{yx} & \sigma^2_{yy} & \sigma^2_{y\psi} \\ \sigma^2_{\psi x} & \sigma^2_{\psi y} & \sigma^2_{\psi\psi} \end{pmatrix} = \begin{pmatrix} 10^{-9} & 0 & 0 \\ 0 & 0.001 & 0 \\ 0 & 0 & 10^{-9} \end{pmatrix}. \quad (22)$$

Finally, the GPS covariances are highly dynamic, being computed online using the *rtklib* software, which processes the u-blox NEO-6P GPS sensor data. Below we present a typical covariance matrix, by averaging the values over a field trial with the robot:

$$\mathbf{R}^{GPS} = \begin{pmatrix} \sigma^2_{xx} & \sigma^2_{xy} & \sigma^2_{xz} \\ \sigma^2_{yx} & \sigma^2_{yy} & \sigma^2_{yz} \\ \sigma^2_{zx} & \sigma^2_{zy} & \sigma^2_{zz} \end{pmatrix} = \begin{pmatrix} 0.00022 & 0.00018 & -0.00012 \\ 0.00018 & 0.00143 & -0.00162 \\ -0.00012 & -0.00162 & 0.00342 \end{pmatrix}. \quad (23)$$

The estimation system uses the available sensors, offering loosely coupled integration of different sources, which can appear and disappear over time.

4.2. Navigation and perception

The FSR Husky leverages from autonomous navigation by following the approach presented in [54], which is available in ROS via the *navigation* metapackage. This way, given any physically reachable goal, the robot should be able to autonomously navigate to that goal, avoiding collisions with obstacles on the way by following a series of steps. The navigation system at the high level is fairly simple: it takes in a navigation goal, data from sensors, and localization information, and outputs velocity commands that are sent to the mobile robot base.

Autonomous navigation of the FSR Husky can be achieved with or without an *a priori* map. Usually in field trials, the robot is initialized without a map, knowing only obstacles that it has perceived with its sensors, and global planning will be fairly optimistic, possibly including areas that it has not yet visited which may traverse unknown space, potentially intersecting unseen obstacles. As more information about the world is acquired, the robot may replan in order to avoid collisions with obstacles. On the other hand, when a static representation of the environment is provided, the robot will follow more informed plans considering distant obstacles.

The navigation algorithm includes several interesting features. For instance, Random Sample Consensus (RANSAC) is applied to filter out Light Detection And Ranging (LIDAR) readings that are invalid due to hardware limitations, such as false positives generated by veiling effects. Also, a planar Costmap, which is initialized with the static map (if available), is used to represent obstacle data and the most recent sensor data, in order to maintain an updated view of the robot's local and global environment. Inflation is performed in 2D to propagate costs from obstacles out to a specified radius in order to conservatively avoid collisions, as illustrated in Fig. 15. The global planner uses an A* algorithm that plans in configuration space computed during obstacle inflation in the Costmap, not taking into account the dynamics or the kinematics of the robot, which are considered instead by the local planner, which generates velocity commands for the robot, safely moving it towards a goal. The planner cost function combines distance to obstacles, distance to the path produced by the global planner, and the speed at

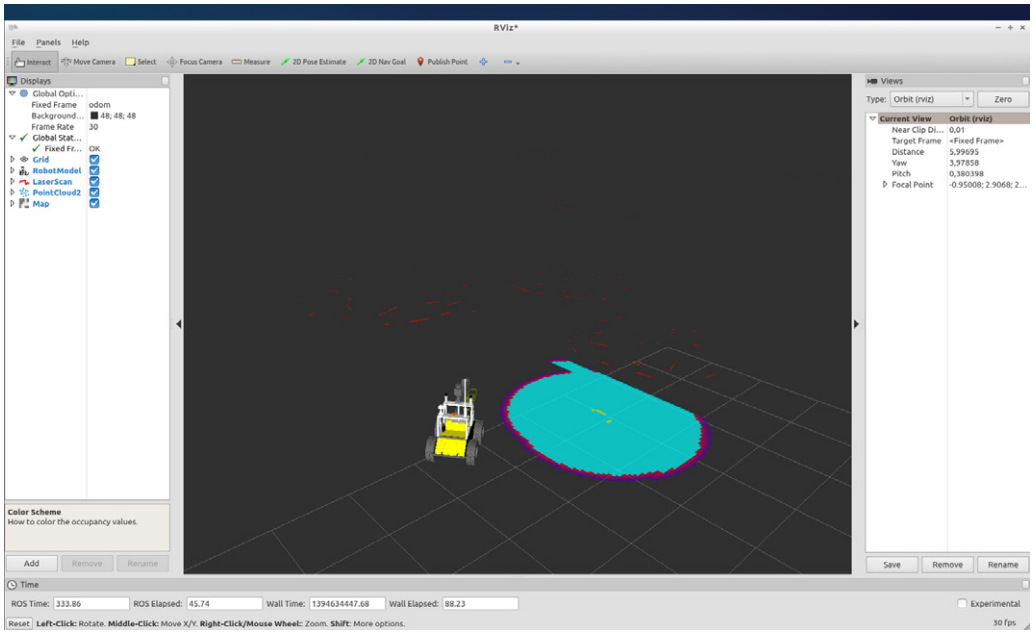

Fig. 15. Inflated obstacle in the robot's local costmap during outdoor autonomous navigation.

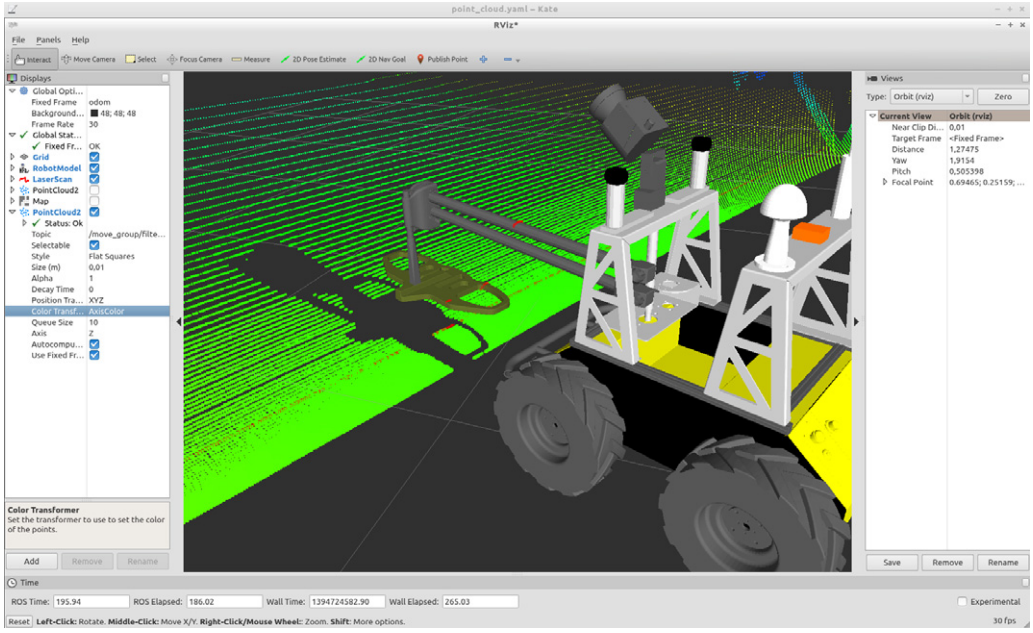

Fig. 16. Point cloud self-filtering.

which the robot travels. Finally, a few recovery behaviors can be performed, *e.g.* due to entrapment. The robot will perform increasingly aggressive behaviors to clear out space around it, and check if the goal is feasible.

Moreover, the FSR Husky can take advantage of its advanced sensor suite to intelligently perceive its surrounding environment. For example, the robot is able to build a 2D map of the environment while navigating within it, using the 20 m range LRF together with a Simultaneous Localization and Mapping (SLAM) approach. In addition, using the PTU unit and the LRF, 3D point clouds of the environment around the robot can be obtained. Note however, that when tilting the PTU, the LRF may "see" the robot's arm, therefore we have implemented a self-filtering system, which is illustrated in Fig. 16. In order to achieve this, each 2D laser scan is converted into a point cloud structure. During this conversion, laser scans are filtered to remove outliers. Afterwards, self filtering is conducted by clearing the points that intersect with the robot's arm. Since the arm may be moving, self filtering is done based on the robot 3D model and the transform to the arm's main frame. Finally, the resulting filtered point cloud is passed to a point cloud assembler module, which fuses all the point clouds obtained in between the extreme positions of the laser while tilting.

The stereo pair of cameras also enables the robot to extract interesting features about its surroundings. In Fig. 17, we show the result of running a feature-based stereo matching algorithm during an outdoor field trial, using frames acquired from the PointGrey Flea3 GigE cameras of the FSR Husky. This was done by running the scale-invariant feature transform (SIFT) algorithm available in OpenCV, which is the primary computer vision library in ROS. In the future, we also intend to use the stereo pair of cameras to perform visual odometry to provide another source of input to our localization system.

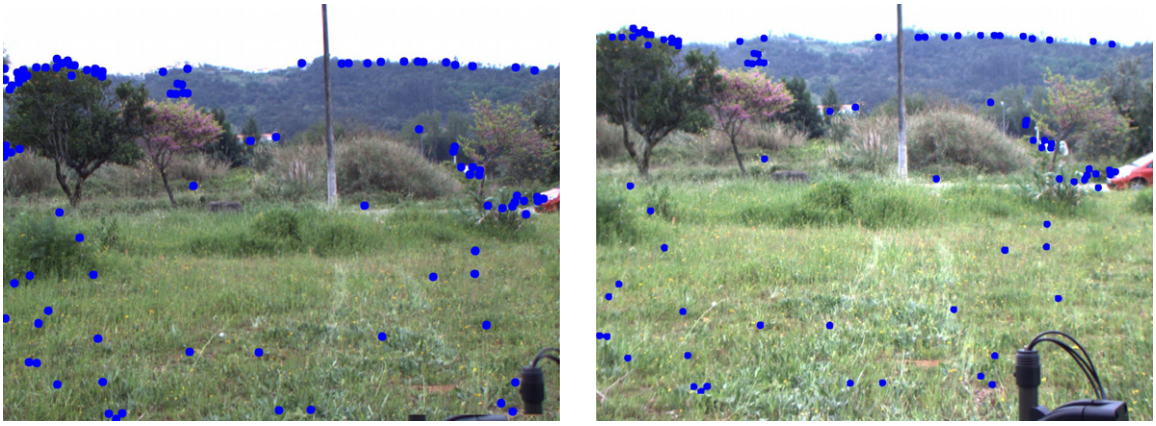

(a) Features in the left camera. (b) Features in the right camera.

Fig. 17. SIFT-based stereo matching in an outdoor field trial.

4.3. Arm control and metal detection

Similarly to robot navigation, it is also crucial to control and perform arm navigation in order to scan the ground for mines. To this end, we have integrated the FSR Husky's mine clearance arm with the *moveit!* mobile manipulation software for ROS [55], which provides planning and trajectory execution functionalities, taking into account the structure and mobility constraints of the 2 DOF arm. Pose goals are continuously sent to the arm during operations in order to guarantee smooth sweeping. Furthermore, using this software arm joints can easily be controlled, as well as sweeping speed and height of the arm.

As referred previously, the MD is mounted on the robotic arm that sweeps the detector above the ground. Pulse Induction MDs send powerful, short pulses of current through a coil of wire about a thousand times per second. Each pulse generates a brief magnetic field. If the metal detector is over a metal object, the pulse creates an opposite magnetic field in the object. When the pulse's magnetic field collapses, causing the reflected pulse, the magnetic field of the object makes it take longer for the reflected pulse to completely disappear. In a pulse induction metal detector, the magnetic fields from target objects affect the reflected pulse, making it last longer than it would in the absence of a metal object. High speed electronics monitor the length of the reflected pulse. By comparing it to the expected length, the circuit can determine if another magnetic field has caused the reflected pulse to take longer to decay. If the decay of the reflected pulse takes more than a few microseconds longer than normal, there is likely a metal object present. Pulse induction detectors do not excel at discriminating type of metal, because the reflected pulse length of various metals are not easily separated. On the other hand, they are useful in many situations in which other metal detector technologies would have difficulty, such as in areas that have highly mineralized soils. Furthermore pulse induction systems can detect metal objects at greater depths when compared to other metal detector technologies.

The Vallon VMP3 metal detector, shown in Fig. 18, aggregates three coils. Each coil outputs 2 channels of raw data plus an alarm channel. Each of the 3 channels is evaluated separately in an analog switched integrator circuit. Those are A/D converted and then filtered in the Digital Signal Processor (DSP), preprocessed and combined to the alarm channel. Soil compensation can be accomplished using the following formula:

$$\text{detection\_alert} = \lambda \cdot \text{ch}_1\text{\_data} + (1 - \lambda) \cdot \text{ch}_2\text{\_data}, \tag{24}$$

where λ is chosen so that detection_alert $= 0$, when no metal samples are present in the soil ($\text{ch}_1\text{\_data} = \text{ch}_1\text{\_zero}$, and $\text{ch}_2\text{\_data} = \text{ch}_2\text{\_zero}$; with $\text{ch}_1\text{\_zero} \neq 0$ and $\text{ch}_2\text{\_ zero} \neq 0$). In order to calculate a signature ϕ of a metal sample, the following formulas are used:

Fig. 18. The original Vallon VMP3, before being modified to fit the arm.

$$\beta = \frac{\text{ch}_2\text{\_data} - \text{ch}_2\text{\_zero}}{\text{ch}_1\text{\_data} - \text{ch}_1\text{\_zero}}, \tag{25}$$

$$\phi = \frac{\beta}{1 - \beta}. \tag{26}$$

Different metals should have different signatures, especially for simple targets. However, in practice, signature values fluctuate especially with complex shaped targets.

In the next section, we conduct experiments to validate the robot's capabilities in an outdoor minefield coverage mission. Furthermore, we provide an overview of the Humanitarian Robotics and Automation Technology Challenge (HRATC 2014), which consisted of several minesweeping trials with the proposed robotic system over long periods of time.

5. Results and discussion

5.1. Coverage of minefields: preliminary work

Area coverage is the problem of sensing all points inside a given space with a certain sensor. In this work we deploy the FSR robot in a bounded minefield and have the robotic arm sweeping continuously the Vallon MD from side to side over the ground. This is done at a constant height in order to sense surrogate mines

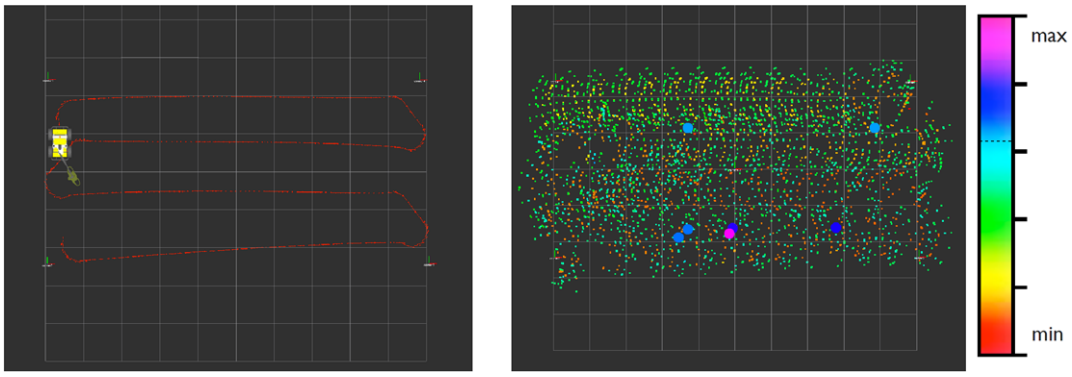

(a) Autonomous coverage trajectory followed by the FSR Husky.

(b) Output of the mine detection module.

Fig. 19. Coverage field trial.

buried in shallow depth. These surrogate mines are composed of a small plastic box with a metal sphere inside with 1 cm of diameter and 5 g of weight. This was chosen accordingly to literature on mines with minimum metallic content found on warzones. The goals of this preliminary test are: (i) evaluate the measurements obtained so as to analyze highly probable location of mines through thresholding; (ii) assess the continuous localization of all modules of the system, composed by detected mines, MD sensor, sweeping arm, and robotic platform; (iii) draw conclusions for an upcoming implementation of minefield coverage strategies with improved terrain traversability, and robust detection against false positives or false negatives in the short-term future.

A two dimensional target area of size 10 × 5 m was defined and marked on the field. The corners of this area are identified by axis labels in the *rviz* window illustrated in Fig. 19(a). The robot was instructed to follow a lawn mowing trajectory autonomously. The arm movement is tracked by the robot, thus the data collected by the MD is indexed in space. This data collected by the MD is pre-processed in order to generate a single scalar representing the amount of metal sensed by the device, as described by (24). We have used this large amount of spatial information to generate a metal distribution map, as depicted in Fig. 19(b). Note that the transformation from the robot's arm polar coordinates acquisitions to a regular Cartesian grid is accomplished by Kriging interpolation [56], a method commonly used in geostatistics. Kriging is based on the notion that the value at an unknown point in space should be the average of the known values at its neighbors weighted by the variogram of the distance to the unknown point. The interpolated distribution map that was generated also shows that complete coverage was accomplished by having the robot follow a lawn mowing trajectory with continuous arm sweeping, as there was no unsearched space left within the target area.

These results validate the autonomous navigation of the robotic platform, whose velocity commands were generated by the simple coverage algorithm tested, as well as the proposed localization system, which in this case used GPS-RTK to provide more precise estimations of the robot's pose, and consequently, arm and MD sensor pose. The integration of the outdoor navigation with the localization system allowed for the accurate trajectory followed by the robot. Furthermore, this experimental trial also validates the mine detecting system. Note that in Fig. 19(b), we have used the hue space color scale to represent the detection values, and those that are superior to the threshold specified by the dashed line in the scale were enlarged for visualization purposes. The *rviz* visualization software for ROS was used to mark in real-time the places where mines are precisely located. The positions given by detections superior to the threshold are consistent with the positions where surrogate mines were buried. Nevertheless, 7 different detections were reported, as illustrated in Fig. 19(b), because 2 pairs of detections are in fact very close spatially. In reality, these were only 2 surrogated mines (instead of 4), out of a total of 5 mines deployed. Therefore, with this technique we have achieved a 100% detection rate plus 2 false positives. It is noteworthy that all surrogate mines are equivalent. However some mines were easier to identify (higher detection certainty) than others. This is due to several factors, such as magnetic properties of the soil, burial depth, and presence of metal fragments in the soil. In addition, significant variations of the detection values within the target area, which are near to the threshold defined, show that a more robust method is necessary to filter out false positive detections.

Although the main focus in this section was the integration of the arm with the robot, and to assess the detection capability provided by the Vallon VMP3 MD, we intend to integrate further detection technologies in the robotic arm. Thus, we are currently evaluating the use of a GPR and an artificial nose for explosive vapor detection, to explore complementary multimodal sensor features, and provide a more robust detection strategy based on probabilistic data fusion. Furthermore, the output of the mine detection system will be taken into account by the navigation module of the robot, thus avoiding triggering the explosive devices.

5.2. An international demining challenge with the FSR Husky

Our research group has been involved in the organization of the Humanitarian Robotics and Automation Technology Challenge (HRATC) 2014 together with IEEE RAS-SIGHT. HRATC is an unprecedented opportunity to enable and engage researchers from around the world to collaborate using their skills and education to benefit humanity, by developing new strategies for autonomous landmine detection using a mobile ground robot. The 2014 edition of HRATC [57] was the first event where teams from around the world participated and tested their autonomous demining strategies remotely on a real world robotic platform, the FSR Husky. A total of 14 teams submitted their entries, and were progressively eliminated based on the stages of the challenge. The grand finale took place at ICRA 2014, Hong Kong, and Coimbra, Portugal remotely.

HRATC consisted of three stages in early 2014: simulation stage, testing stage, and challenge stage. For the simulation stage, the Gazebo 3D simulator described in Section 3.6 was adopted. This is run in a Linux-based Operating System, using ROS for controlling the virtual robot. Using this framework, the teams were classified according to the performance of their strategy in a simulation scenario. The scoring metric was computed using several performance measures that included number of detected mines, number

Fig. 20. HRATC 2014 apparatus and competition venue at the University of Coimbra.

of exploded mines, covered area, and coverage time. The best-ranked teams were then allowed to advance to the testing phase. In the testing phase, the teams ran their detection and classification strategies using ROS on the FSR Husky robot in an outdoor arena covered by low grass, ditches and surrogate mines. The tests occurred during three weeks of May 2014, and each team had three trials to evaluate and adjust their strategy. After the third trial, four teams have participated in the finals at ICRA 2014, consisting of two final runs in May 31, and June 1, which were video-streamed live over the internet from Coimbra, Portugal. The final competition environment was an open wood area with a size of 10×5 m, as shown in Fig. 20, and delimited by 4 GPS coordinates. The competition area was marked by plastic tape for visualization purposes, and a virtual fence was deployed to stop the robots from going outside the competition area. Surrogate mines were buried in the field, along with other metal debris (coke cans, metal pieces and large screws), and the teams were evaluated according to the scoring metric presented below:

$$Score\ (\%) = 80\,DS + 5\,TS + 15\,CR, \tag{27}$$

where:

$$DS = \frac{DM \cdot (1 - {}^{EKM}/_{TM} - 0.5\,{}^{EUM}/_{TM})}{DM + UCA + 0.5\,UUA + WMD}, \tag{28}$$

$$TS = 1 - {}^{TT}/_{1800}, \tag{29}$$

$$CR = \frac{AC}{TA}. \tag{30}$$

In the scoring formula, DS, TS and CR have values ranging from 0 to 1, and they represent the detection score, time score and coverage ratio. Furthermore, DM is the number of detected mines, EKM is the number of exploded known mines, EUM is the number of exploded unknown mines, TM is the total number of mines, UCA stands for the undetected mines in the covered area (false negatives), UUA stands for the undetected mines in the uncovered area, and WDM are the number of wrongly detected mines (false positives). Finally, TT is the total time in seconds with maximum value of 1800, *i.e.* 30 min, AC is the area covered, and TA is the total area. Both AC and TA are represented in square-meters.

In order to compute the score of each team automatically, the judge framework was developed by members of the organization from the Federal University of Rio Grande do Sul, Brazil (*cf.* Fig. 21).

During the challenge, every team had the opportunity to make use of all the robot's sensors described previously in this paper, as they seem fit, in order to develop their own mine detection algorithm. Furthermore, we also provided data in real-time from the precise localization system developed (*cf.* Section 4.1), a dataset for the teams to assess the behavior of the MD over different types of soil, optimized parameters for arm sweeping with our robot, and several examples on how to control the robot in ROS. In general, the challenge resulted in numerous trials with the FSR Husky, which was continuously tested for long periods of time in the field.[7]

Fig. 21 illustrates the best trial of each team that participated in the finals. The team Across displayed a very erratic approach, as shown by the robot trajectory in Fig. 21(a). The US Miners team quickly finished the trial (highest TS), however with several wrong detections and a mine explosion (*cf.* Fig. 21(b)). The Geeks of the Square Table team presented the best coverage approach (highest CR) by following a lawn mowing trajectory with the robot, as seen in Fig. 21(c). However they were not able to successfully detect any of the surrogated mines. Finally, the team Orion used a spiral coverage approach from the center of the field to the outside (see Fig. 21(d)), being the only team that successfully detected a mine (highest DS). Thus, they have won the challenge with a highest score of 17.19%.

Despite the successful use of the robot by the teams in the HRATC 2014 Challenge, especially in terms of robot navigation in the field and arm control, the winning approach was still far from full success, given that only one of the five mines were correctly detected by the grand winner. This shows that there is much room to improve in next year's challenge. Namely, the teams may need more time to prepare the challenge, ROS expertise is highly advised, the teams may benefit from a longer testing stage with the robot in the field before the finals, and possibly from additional datasets with the mine detection system so as to further understand how to correctly identify mines.

The three best-ranked teams received a cash prize together with a certificate and a plaque. During the competition, important lessons for the organizing team were also learned, which allows us to plan future developments with the robot.

First of all, the time between arriving to the field and starting the tests is usually around 30–45 min. This happens due to the technical equipment that is necessary to carry and setup when conducting field trials (*e.g.* GPS-RTK station, base station computer, WiFi, etc.), and because the FSR Husky is a complex system, so it is necessary to guarantee that all independent components will work in unison during robot operation. In order to address this issue we plan to develop a simple and intuitive graphical user interface

[7] Several footage of the finals are available at: http://isr.uc.pt/HRATC2014/Movies.

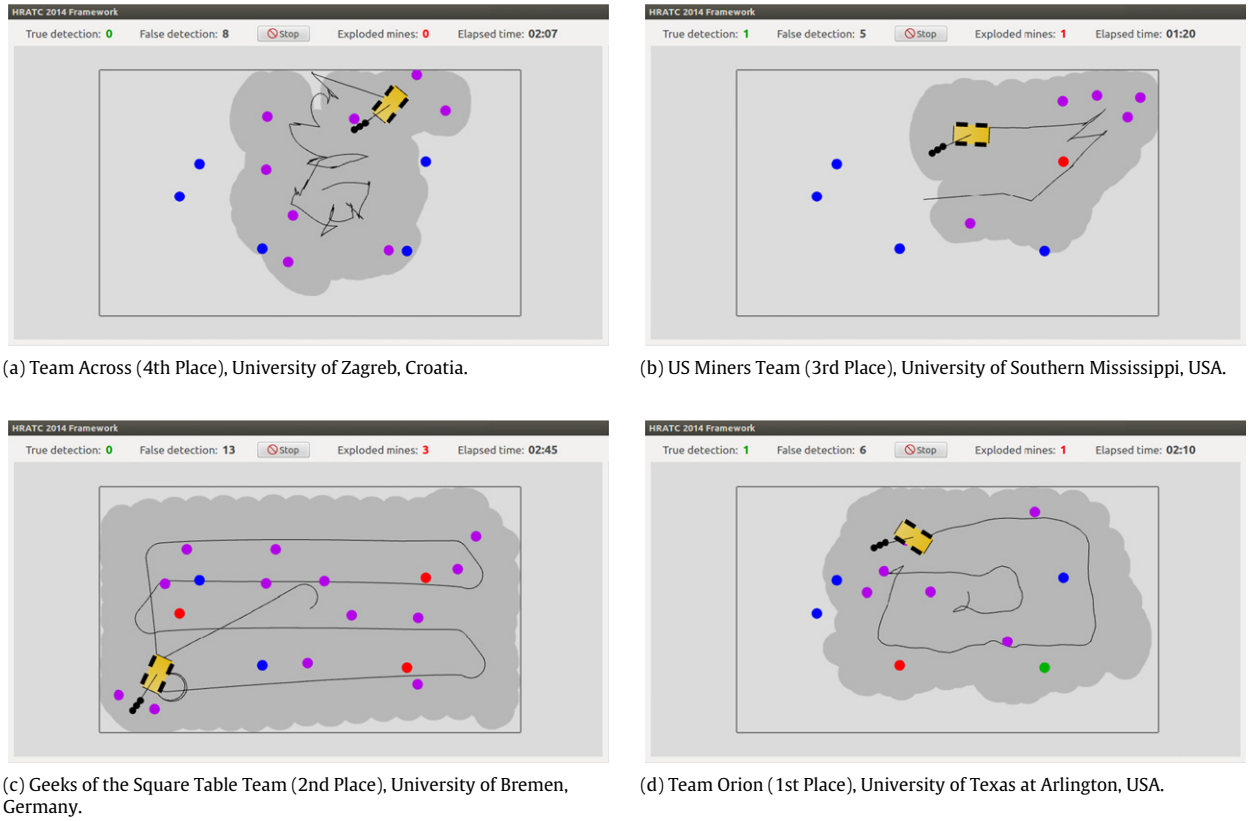

(a) Team Across (4th Place), University of Zagreb, Croatia.

(b) US Miners Team (3rd Place), University of Southern Mississippi, USA.

(c) Geeks of the Square Table Team (2nd Place), University of Bremen, Germany.

(d) Team Orion (1st Place), University of Texas at Arlington, USA.

Fig. 21. HRATC 2014 judge framework used to evaluate the performance of the competitors. Blue circles represent undetected mines, red circles represent mines that exploded, green circles represent mines that were successfully detected, and purple circles represent false detections. (For interpretation of the references to color in this figure legend, the reader is referred to the web version of this article.)

(GUI), which should provide in real-time the status of all the hardware and sensors within the robot. Furthermore, the arm localization may accumulate error due to steps skipped by the stepper motor, when the robot traverses rough terrains or rotates very quickly. In extreme situations, these skipped steps may result in the arm stopping as a security measure, due to surpassing the range of rotation imposed by the limit switch. Similarly, in such situations the PTU suffers from vibrations, which highly affects the readings reported by the SICK LMS111 laser. We plan to replace the main motor and test a more stable tilting unit in order to conduct further tests. Also concerning the mine clearance arm, we observed that the Nanotec PD4-N60 motor is not always reliable, and may crash during operation. As a direct consequence of this, the arm often halts and will not react to further commands. When this situation occurs, it is necessary to reset the robot, since the power supply is common for both sources. In the future, we plan to decouple the arm power, by adding a power switch to reset it if necessary, without affecting the remaining sensors. Moreover, we feel that the testing stage before the finals was crucial, because there are a few aspects that are slightly different between the simulation and the real robot. More specifically, the localization system and the arm control is not exactly mimicked in the simulation framework. The testing stage allowed the participants to realize these differences and adjust their strategies accordingly. Perhaps, an in-depth study of the localization conditions and arm control on the real robot will allow a more correct parametrization of the simulation framework.

It is our belief that it is very important to promote humanitarian causes by leveraging existing and emerging technologies for the benefit of humanity and towards increasing the quality of life in underserved, underdeveloped areas in collaboration with global communities and organizations. Thus, following this philosophy, humanitarian challenges such as the one mentioned can progressively change the world by addressing the global emergency that humanitarian demining represents. In this submission, we provide an overview video of the 2014 edition of HRATC.[8]

6. Conclusion and future work

In this article we have presented the FSR Husky, an all terrain demining platform developed in the framework of the EU FP7 TIRAMISU project. The implementation of our robotic system was motivated by the need to increase safety in humanitarian demining missions, following at the same time three important design goals: being affordable, lightweight and autonomous. The implementation, features, and modular integration of the robotic system were described, focusing especially on its steering base, hardware and sensors, robot kinematics and constraints, energy consumption, arm sweeping for mine coverage, software, and testing tools. In addition, details on its current capabilities such as outdoor localization, navigation, environment perception and mine detection were presented. Finally, outdoor field trials were carried out to validate the robot functionalities and report continuous work in progress on autonomous landmine detection. Several hours of field runs with the robot allowed for a discussion of lessons learned during the periods of test, and to plan future development.

As described along the article, several directions of research are foreseen in the near future. We would like to further characterize our metal detection system by inspecting the influence of target content, sweeping speed, and distance from the target in the probability of detection. We also plan to integrate a GPR with the MD, and explore sensor fusion methods to increase the reliability of our mine detection system. Additionally, we would like to further

[8] HRATC 2014 lookback: https://www.youtube.com/watch?v=13xPoXWACJo.

explore the stereo pair of cameras available in the robot to provide visual odometry estimates to our localization system, as well as fusing the incoming data from the cameras with the laser point clouds in order to generate an RGB-D 3D reconstruction of the environment. This will be useful to assess the traversability of outdoor field scenarios, which in turn may represent an important component for the robot's navigation system, and will allow us to test the robot in even more challenging conditions, *e.g.* with steep ramps, diversified obstacles, and abrupt terrain. Even though we have validated the navigation and detection system in a minefield coverage experiment, in order to have a full solution it is necessary that the robot takes the mine position into account, integrate it as a virtual obstacle during autonomous navigation, and replan its trajectory in order to avoid the detonation of the mine [58]. Additionally, the robot should have a marking mechanism to visibly identify mines detected in the field. Finally, we plan to compare different coverage approaches in terms of the FSR Husky's power consumption, in order to extract energy-efficient strategies for minefield coverage.

Acknowledgments

This work was partially carried out in the framework of TIRAMISU project (www.fp7-tiramisu.eu). This project is funded by the European Community's Seventh Framework Program (FP7/SEC/284747). The authors gratefully acknowledge Clearpath Robotics, Inc.

Appendix. Terminology

Acronym	Description
AC	Area Covered
AP	Anti-Personnel
CARMEN	Carnegie Mellon Robot Navigation Toolkit
CPU	Central Processing Unit
CR	Coverage Ratio
DC	Direct Current
DEEC	Department of Electrical Engineering and Computers
DM	Detected Mines
DOF	Degrees of Freedom
DS	Detection Score
DSP	Digital Signal Processor
EDMS	Elevated Device Mounting Structure
EKF	Extended Kalmand Filter
EKM	Exploded Known Mines
EOD	Explosive Ordnance Disposal
EU	European Union
EUM	Exploded Unknown Mines
FNA	Fast Neutron Analysis
FOV	Field of View
FP7	7th Framework Programme for Research and Technological Development
FPS	Frames per Second
FSR	Field and Service Robotics
GigE	Gigabit Ethernet
GPR	Ground Penetrating Radar
GPS	Global Positioning System
GUI	Graphical User Interface
HRATC 2014	Humanitarian Robotics and Automation Technology Challenge 2014
HMI	Human–Machine Interaction
ICR	Instantaneous Center of Rotation
ICRA 2014	International Conference on Robotica and Automation 2014
IEEE	Institute of Electrical and Electronics Engineers
IMU	Inertial Measurement Unit
IP	International Protection
ISR	Institute of Systems and Robotics
KF	Kalman Filter
LIDAR	Light Detection And Ranging
LOCOSTRA	Low Cost Tractor for Humanitartian Demining
LRF	Laser Range Finder
MD	Metal Detector
MRS	Multi-Robot Systems
NMEA	National Marine Electronics Association
NQR	Nuclear Quadropole Resonance
OpenCV	Open Source Computer Vision
PEMEX	Personal Mine Explorer
PPP	Precise Point Positioning
PTU	Pan and Tilt Unit
RAM	Random Access Memory
RANSAC	Random Sample Consensus
RAS-SIGHT	Robotics and Automation Society—Special Interest Group on Humanitarian Technology
RGB-D	Red, Green, Blue, Depth
RMA	Royal Military Academy
ROS	Robot Operating System
RTK	Real-Time Kinematic
SIFT	Scale-Invariant Feature Transform
SLAM	Simultaneous Localization and Mapping
SSD	Solid-State Disk
SPU	Single Processing Unit
TA	Total Area
TOF	Time of Flight
TIRAMISU	Toolbox Implementation for Removal of Anti-Personnel Mines, Submunitions and UXO
TM	Total Number of Mines
TNA	Thermal Neutron Analysis
TNT	Trinitrotoluene
TS	Time Score
TT	Total Time
UAV	Unmanned Aerial Vehicle
UC	University of Coimbra
UCA	Undetected mines in Covered Area
UGV	Unmanned Ground Vehicle
USV	Unmanned Surface Vehicle
UUA	Undetected mines in Uncovered Area
UNICEF	United Nations Children's Fund
USB	Universal Serial Bus
UXO	Unexploded Ordnance
WDM	Wrongly Detected Mines
XEE	Xsens Estimation Engine

References

[1] Y. Baudoin, M.K. Habib, Using robots in Hazardous Environments: Landmine Detection, De-Mining and Other Applications, Woodhead Publishing in Mechanical Engineering, 2011.
[2] D. Portugal, L. Marques, M. Armada, Deploying field robots for humanitarian demining: Challenges, requirements and research trends, in: Mobile Service Robotics: 17th International Conference on Climbing and Walking Robots (CLAWAR 2014) and the Support Technologies for Mobile Machines, World Scientific Publishing, 2014, pp. 649–656.
[3] H. Herman, D. Few, R. Versteeg, J. Valois, J. McMahill, M. Licitra, E. Henciak, Modular countermine payload for small robots, in; Proc. of the SPIE: Detection and Sensing of Mines, Explosive Objects, and Obscured Targets XV, Vol. 7664, April 5–9, Orlando, FL, USA, 2010.
[4] T. Ueno, K. Amemiya, M. Ikuta, O. Nishino, Mine-clearing system for use in international peacekeeping, Hitachi Rev. 62 (3) (2013).
[5] C.S. Rathnayake, Participatory Web GIS for real time demining mapping with GPS enabled remotely controlled platforms, in: Proc. of the 8th Annual Asian Conference & Exhibition on Geospatial Information, Technology and Applications, Map Asia 2009, August 18–20, Singapore, 2009.
[6] M.K. Habib, Humanitarian demining: the problem, difficulties, priorities, demining technology and the challenge for robotics, in: Humanitarian Demining, I-Tech Education and Publishing, 2008.

[7] S. Singh, M. Freese, J.P. Trevelvan, Field characterization of humanitarian demining for future robotic assessment, in: Proc. of the IEEE International Conference on Robotics and Automation, ICRA 2007, Workshop on Robotics in Challenging and Hazardous Environments, Rome, Italy, 2007.
[8] A.M. Kaneko, M. Marino, E.F. Fukushima, Humanitarian demining robot gryphon: new vision techniques and optimization methods, in: Proc. of the IEEE/RSJ International Conference on Intelligent Robots and Systems, IROS 2010, October 18–22, Taipei, Taiwan, 2010.
[9] E.F. Fukushima, M. Freese, T. Matsuzawa, Humanitarian demining robot gryphon—current status and an objective evaluation, Int. J. Smart Sens. Intell. Syst. 1 (3) (2008).
[10] E.E. Cepolina, Sustainable and appropriate technologies for humanitarian demining, in: Using Robots in Hazardous Environments, Woodhead Publishing in Mechanical Engineering, 2011.
[11] E.E. Cepolina, Appropriate technologies in humanitarian demining: Potential impact of participatory re-designed agricultural machines and tools, in: The 8th IARP Workshop on Humanitarian Demining, HUDEM 2010, April 27–29, Šibenik, Croatia, 2010.
[12] H. Balta, G. de Cubber, D. Doroftei, Y. Baudoin, H. Sahli, Terrain traversability analysis for off-road robots using time-of-flight 3D sensing, in: Proc. of the 7th IARP RISE Robotics for Risky Environments—Extreme Robotics Workshop, October 1–3, Saint-Petersburg, Russia, 2013.
[13] A. Conduraru, I. Conduraru, G. Asachi, E. Puscalau, G. de Cubber, D. Doroftei, H. Balta, Development of an autonomous rough-terrain robot, in: Proc. of the IEEE/RSJ International Conference on Intelligent Robots and Systems, IROS 2012, Workshop on Robotics for Environmental Monitoring, October 7–12, Vilamoura, Algarve, Portugal, 2012.
[14] J.D. Nicoud, M.K. Habib, The Pemex-B autonomous demining robot: perception and navigation strategies, in: Proc. of the IEEE/RSJ International Conference on Intelligent Robots and Systems, IROS 1995, August 5–9, Pittsburgh, PA, USA, 1995.
[15] P. Santana, C. Cândido, P. Santos, L. Almeida, L. Correia, J. Barata, The ares robot: Case study of an affordable service robot, in: European Robotics Symposium 2008, Vol. 44, Springer, 2008, pp. 33–42.
[16] A. Irawan, K. Nonami, Optimal impedance control based on body inertia for a hydraulically driven hexapod robot walking on uneven and extremely soft terrain, J. Field Robot. 28 (3) (2011) 424–440.
[17] P. Gonzalez de Santos, J.A. Cobano, E. Garcia, J. Estremera, M. Armada, A six-legged robot-based system for humanitarian demining missions, Mechatronics 17 (2007) 417–430. Elsevier.
[18] P. Debenest, E.F. Fukushima, Y. Tojo, S. Hirose, A new approach to humanitarian demining part 1: Mobile platform for operation on unstructured terrain, Auton. Robots 18 (2005) 303–321. Springer.
[19] R. Bogue, Detecting mines and IEDs: what are the prospects for robots? Ind. Robot: Int. J. 38 (5) (2011) 456–460.
[20] P. Rudakevych, S. Clark, J. Wallace, Integration of the fido explosives detector onto the PackBot EOD UGV, in: Proc. of the SPIE: Unmanned Systems Technology IX, Vol. 6561, April 9–12, Orlando, FL, USA, 2007.
[21] C. Lundberg, H. Christensen, R. Reinhold, Long-term study of a portable field robot in urban terrain, J. Field Robot. 24 (8–9) (2007) 625–650.
[22] B. Christensen, W. Drotning, S. Thunborg, Model-based, sensor-directed remediation of underground storage tanks, J. Robot. Syst. 9 (2) (1992) 145–159.
[23] S.B. Suh, J.H. Choi, C.H. Cho, Y.S. Jin, S.Y. Hyun, S. Kang, Mine detecting robot system, in: Field and Service Robotics, in: Springer Tracts in Advanced Robotics Series, vol. 92, Springer, Heidelberg, New York, 2014.
[24] K. Takahashi, H. Preetz, J. Igel, Soil properties and performance of landmine detection by metal detector and ground-penetrating radar—soil characterisation and its verification by a field test, J. Appl. Geophys. 73 (4) (2011) 368–377. Elsevier.
[25] P. Valpolini, IED detection: Oh Blast!, Armada Int. 34 (3) (2010) 24–30.
[26] J. Prado, G. Cabrita, L. Marques, Bayesian sensor fusion for landmine detection using a dual-sensor hand-held device, in: Proc. of the 39th Annual Conf. of the Annual Conference of IEEE Industrial Electronics Society, IECON 2013, Vienna, Austria, 2013.
[27] M. Sato, Deployment of GPR system ALIS for humanitarian demining in cambodia, in: Proc. of the 13th International Conference on Ground Penetrating Radar, GPR 2010, June 21–25, Lecce, Italy, 2010.
[28] C. Bruschini, K. De Bruyn, H. Sahli, J. Cornelis, Study on the sate of the art in the EU related to humanitarian demining technology, products and practice. EUDEM: The EU in Humanitarian Demining—Final Project Report, July, Brussels, Belgium, 1999.
[29] Y. Baudoin, TIRAMISU: FP7-project for an integrated toolbox in humanitarian demining, focus on UGV, UAV, technical survey and close-in detection, in: Proc. of the International Conference on Climbing and Walking Robots, CLAWAR 2013, Sydney, Australia, July 14–17, 2013.
[30] E. Galceran, M. Carreras, A survey on coverage path planning for robotics, Robot. Auton. Syst. 61 (2013) 1258–1276.
[31] H. Choset, Coverage for robotics—a survey of recent results, Ann. Math. Artif. Intell. 31 (1–4) (2001) 113–126. Springer.
[32] J. Jin, L. Tang, Coverage path planning on three-dimensional terrain for arable farming, J. Field Robot. 28 (5) (2011) 690–713.
[33] T. Oksanen, A. Visala, Coverage path planning algorithms for agricultural field machines, J. Field Robot. 26 (8) (2009) 651–668.
[34] P. Dasgupta, A. Muñoz-Meléndez, K.R. Guruprasad, Multi-robot terrain coverage and task allocation for autonomous detection of landmines, in: Proc. of the SPIE: Sensors, and Command, Control, Communications, and Intelligence (C3I) Technologies for Homeland Security and Homeland Defense XI, Vol. 8359, April 23–25, Baltimore, MD, USA, 2012.
[35] D. Portugal, R.P. Rocha, Distributed multi-robot patrol: a scalable and fault-tolerant framework, Robot. Auton. Syst. 61 (12) (2013) 1572–1587.
[36] S. Wirth, P.L. Negre Carrasco, G.O. Codina, Visual odometry for autonomous underwater vehicles, in: Proc. of the MTS/IEEE OCEANS, Bergen, Norway, June 10–13, 2013.
[37] J.L. Martínez, A. Mandow, J. Morales, S. Pedraza, A.J. García-Cerezo, Approximating kinematics for tracked mobile robots, Int. J. Robot. Res. 24 (10) (2005) 867–878.
[38] J. Pentzer, S. Brennan, Model-based prediction of skid-steer robot kinematics using online estimation of track instantaneous centers of rotation, J. Field Robot. 31 (3) (2014) 455–476.
[39] A. Mandow, J.L. Martínez, J. Morales, J.L. Blanco, Experimental kinematics for wheeled skid-steer mobile robots, in: Proc. of the IEEE/RSJ International Conference on Intelligent Robots and Systems, IROS 2007, Diego, California, USA, October 29–November 2, 2007.
[40] M.P. Kazmierkowski, R. Krishnan, F. Blaabjerg, J.D. Irwin, Control in Power Electronics: Selected Problems, in: Academic Press Series in Engineering, 2002.
[41] J. Tal, Speed control by phase-locked servo systems–new possibilities and limitations, IEEE Trans. Ind. Electron. Control Instrum. (1) (1977) 118–125.
[42] M. Furlan, A. Cernigoj, M. Boltezar, A coupled electromagnetic-mechanical-acoustic model of a DC electric motor, COMPEL 22 (4) (2003) 1155–1165.
[43] F. Jansen, T. Nielsen, Bayesian Networks and Decision Graphs, second ed., Springer Verlag, 2007.
[44] A.M. Lewis, T.J. Bloodworth, D.M. Guelle, F.R. Littmann, A. Logreco, M.A. Pike, Systematic Test & Evaluation of Metal Detectors (STEMD). Interim Report Laboratory Tests Italy, Institute for the Protection and Security of the Citizen, 2006.
[45] M. Quigley, B. Gerkey, K. Conley, J. Faust, T. Foote, J. Leibs, E. Berger, R. Wheeler, A. Ng, ROS: an open-source robot operating system, in: Proceedings of the IEEE International Conference on Robotics and Automation, ICRA 2009, Workshop On Open Source Software, May 12–17, Kobe, Japan, 2009.
[46] A. Araújo, D. Portugal, M.S. Couceiro, R.P. Rocha, Integrating arduino-based educational mobile robots in ROS, J. Intell. Robot. Syst. (2014) Special Issue on Autonomous Robot Systems, Springer.
[47] B. Gerkey, R. Vaughan, A. Howard, The player/stage project: tools for multi-robot and distributed sensor systems, in: Proceedings of the Intelligent Conference on Advanced Robotics, ICAR 2003, 317–323, Coimbra, Portugal, 2003.
[48] M. Montemerlo, N. Roy, S. Thrun, Perspectives on standardization in mobile robot programming: the carneggie mellon navigation (CARMEN) toolkit, in: Proceedings of the 2003 IEEE/RSJ International Conference on Intelligent Robots and Systems, IROS 2003, Las Vegas, Nevada, October, 2003.
[49] R. Vaughan, Massively multi-robot simulation in stage, J. Swarm Intell. 2 (2–4) (2008) 189–208. Springer.
[50] N. Koenig, A. Howard, Design and use paradigms for Gazebo, an open-source multi-robot simulator, in: Proceedings of the 2004 IEEE/RSJ International Conference on Intelligent Robots and Systems, IROS 2004, 2149–2159, Sendai, Japan, September 28–October 2, 2004.
[51] G. Bradski, A. Kaehler, Learning OpenCV: Computer vision with the OpenCV Library, O'Reilly Media, 2008.
[52] M.S. Grewal, L.R. Weill, A.P. Andrews, Global Positioning Systems, Inertial Navigation and Integration, second ed., John Wiley & Sons, 2007.
[53] J.B. Tsui, Fundamentals of Global Positioning Systems Receivers: A Software Approach, second ed., John Wiley & Sons, 2005.
[54] E. Marder-Eppstein, E. Berger, T. Foote, B. Gerkey, K. Konolige, The office marathon: robust navigation in an indoor office environment, in: Proceedings of the 2010 IEEE International Conference on Robotics and Automation, ICRA 2010, May 3–8, Anchorage, Alaska, USA, 2010.
[55] I.A. Sucan, S. Chitta, MoveIt!, 2014. Available Online: http://moveit.ros.org.
[56] D.M. Hawkins, N. Cressie, Robust kriging—a proposal, J. Int. Assoc. Math. Geol. 16 (1) (1984) 3–18.
[57] R. Madhavan, L. Marques, E. Prestes, P. Dasgupta, G. Cabrita, D. Portugal, B. Gouveia, V. Jorge, R. Maffei, G. Franco, J. Garcia, 2014 humanitarian robotics and automation technology challenge, IEEE Robot. Autom. Mag. 21 (3) (2014) 10–16. IEEE.
[58] K. Jensen, L.B. Larsen, K.S. Olsen, J. Hansen, R.N. Jørgensen, First results: robot mapping of areas contaminated by landmines and unexploded ordnance, in: Proc. of the 10th IARP Workshop on Humanitarian Demining, HUDEM 2012, April 24–26, Šibenik, Croatia, 2012.

David Portugal is a Post-Doctoral Researcher at the Institute of Systems and Robotics (ISR) of the University of Coimbra (UC), Portugal. Currently, he conducts active research in the European Union-funded project TIRAMISU within the FP7 framework, which deals with the development of a toolbox to assist Humanitarian Demining, being specially focused on robotic technology to promote peace, security, conflict prevention and post-conflict reconstruction. He holds an M.Sc. degree in Electrical Engineering and Computers from the Faculty of Sciences and Technology of the University of Coimbra obtained in September, 2009 and a Ph.D. degree in Robotics and Automation from the same university in March, 2014. His research interests include cooperative robotics, field robotics, multi-agent systems, meta-heuristics and optimization.

Gonçalo Cabrita is a Doctoral Candidate on Electrical and Computer Engineering at the University of Coimbra and a researcher at the Institute of Systems and Robotics (ISR), University of Coimbra, Portugal. His Ph.D. studies are focused on mobile robot olfaction and exploration, environmental monitoring, odor plume detection and odor source localization. He also holds an M.Sc. degree in Electrical Engineering and Computers obtained in 2009. During his Ph.D., he has worked as a fellow within the European Project GUARDIANS and he is currently collaborating in the European FP7 Project TIRAMISU within the FP7 framework, with particular focus on sensor fusion for landmine detection.

Bruno Duarte Gouveia is a Researcher at the Institute of Systems and Robotics (ISR) of the University of Coimbra (UC), Portugal. Currently, he conducts active research in the European Union-funded project TIRAMISU within the FP7 framework. He is also pursuing a M.Sc. degree in Informatics Engineering from the Faculty of Sciences and Technology of the University of Coimbra, and his research interests include distributed systems, parallel computing, service robotics and simultaneous localization and mapping.

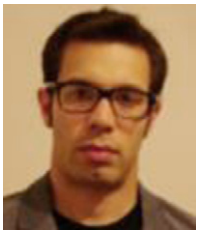

David Costa Santos is a Researcher at the Institute of Systems and Robotics (ISR) in Coimbra, Portugal. He holds an M.Sc. degree in Mechanical Engineering from the University of Coimbra, obtained in 2013. His Master's Thesis focused on Carbon Nanotubes and Composite Materials. Currently, he conducts active research in the European Union-funded project TIRAMISU within the FP7 framework. His main research interests include mechanical design, dimensioning and prototyping, and development of innovative and disruptive solutions for anti-personnel landmines detection.

José Augusto Prado completed his Bachelor degree in Computer Science at University Positivo in Paraná (Brazil) in 2002, the M.Sc. degree in Computer Science and Probabilistic Algorithms at the Federal University of Paraná (Brazil) in 2005, and the Ph.D.degree in Robotics and Automation at the University of Coimbra (Portugal) in 2012. During his Ph.D. he worked as a fellow within the European Project BACS (Contract no. FP6-IST-027140), and afterwards he was sponsored by a scholarship from the Portuguese Foundation for Technology and Sciences. In his thesis, studies about human robot interaction were performed while focusing on Bayesian approaches for robotic perception and sensor fusion. He has participated and contributed to several European Projects such as: BACS (Bayesian Approach for Cognitive Systems), SocialRobot, and TIRAMISU. He is currently integrated as a Post-Doctoral fellow in the Field Robotics research group, within the Institute of Systems and Robotics (ISR-UC).